2017

Biphasic Cellulose Acetate/Rtil Membranes And Functionalized Graphene Adsorbents For Natural Gas Processing: Experimental And Molecular Simulation Studies

Amir Khakpay
University of Mississippi

BIPHASIC CELLULOSE ACETATE/RTIL MEMBRANES AND FUNCTIONALIZED GRAPHENE ADSORBENTS FOR NATURAL GAS PROCESSING: EXPERIMENTAL AND MOLECULAR SIMULATION STUDIES

A Dissertation
presented in partial fulfillment of requirements
for the degree of Doctor of Philosophy
in the Department of Chemical Engineering
The University of Mississippi

by

AMIR KHAKPAY

December 2017

ABSTRACT

In this dissertation, gas separation using membranes is investigated for natural gas upgrading. The main objectives of this study are separation of high value hydrocarbons such as propane (C_3H_8) from natural gas and carbon dioxide (CO_2) separation from light gases such as nitrogen (N_2) and methane (CH_4). To achieve these goals, supported ionic liquid membranes (SILMs), biphasic membranes, and nanoporous graphene (NPG) and graphene oxide (NPGO) membranes are studied.

Biphasic membranes are proposed to overcome SILMs issues for gas separation. The major issues with SILMs are low room temperature ionic liquid (RTIL) content and instability at high cross-membrane pressure. For this purpose, single and biphasic cellulose acetate (CA)/[emim][SCN] membranes were fabricated using the solution casting and solution casting/phase inversion methods, respectively. Infrared spectra and atomic force micrographs were generated to characterize the fabricated membranes. Moreover, the transport properties of CO_2, N_2, CH_4, and C_3H_8 gases through the CA/[emim][SCN] dope membrane (single phase), cast biphasic CA/[emim][SCN] membrane, and supported [emim][SCN] membrane were determined using a batch gas permeance system and a continuous flow instrument. The results indicate that the SILM has the highest and the dope membrane has the lowest permeability for CO_2 and C_3H_8. The cast biphasic membrane and SILM give almost similar permeabilities for these gases. The stability of the dope, biphasic, and SILM membranes are further determined, indicating there is a breakthrough point for all membranes. This point for the biphasic and SILM membranes

corresponds to a similar pressure. This shows that biphasic membranes have potential to compete with SILMs for gas separation applications by improving casting procedure. The dope membrane is less stable at high pressures than the biphasic and SILM membranes, since it is in liquid state.

Molecular dynamics simulations were performed to gain fundamental molecular insights on the concentration-dependent adsorption and gas transport properties of the components in a CH_4/CO_2 gaseous mixture in single- and double-layered nanoporous graphene (NPG) and graphene oxide (NPGO) separation platforms. While these platforms are promising for a variety of separation applications, much about the relevant gas separation mechanisms in these systems is still unexplored. Based on the gas adsorption results in this work, at least two layers of CO_2 are formed on the gas side of both NPG and NPGO, while no adsorption is observed for pure CH_4 on the single-layered NPG. In contrast, increasing the CH_4 concentration in the CH_4/CO_2 mixture leads to an enhancement of the CH_4 adsorption on both separation platforms. The through-the-pore diffusion coefficients of both CO_2 and CH_4 increase with an increase in the CH_4 concentration for all NPG and NPGO systems. The permeance of CO_2 is smaller than that of CH_4, suggesting the NPG and NPGO platforms are more suitable as CO_2 adsorbents or membranes for the CH_4/CO_2 (rather than the CO_2/CH_4) separation. The highest observed selectivities for the CH_4/CO_2 separation in the NPG and NPGO platforms are about 5 and 6, respectively.

TABLE OF CONTENTS

LIST OF FIGURES

LIST OF TABLES

CHAPTER I

INTRODUCTION

Natural gas as a main energy source is attracting more attention due to its lower price than that of oil. Furthermore, the natural gas emits 50 to 60 percent less greenhouse gases to the atmosphere when compared to fuels such as coal [1]. Therefore, the natural gas processing to remove the undesired components is also gaining more attention. Natural gas mainly contains CH_4, ethane, CO_2, N_2, and some higher hydrocarbons such as C_3H_8 and C_4H_{10} [2].

In this dissertation, gas separation using novel membranes are investigated. The main objective of this work is to explore novel membranes for natural gas upgrading. The main goal of most studies is to remove CO_2 from natural gas. Several types of membranes such as polymeric membranes and zeolite membranes have been developed. However, the application of current membranes is limited due to low selectivities at high permeabilities. In addition, separation of C_3H_8 and C_4H_{10} from natural gas requires reverse-selective membranes to compete with the cryogenic separation [3]. C_3H_8 and C_4H_{10} can be used as a feed in the petrochemical industry. Room temperature ionic liquid (RTIL) based membranes or RTIL-membranes have potential to be reverse-selective membranes for the separation of C_3H_8 and C_4H_{10} from natural gas because solubility dominates their gas transport [3]. Furthermore, RTIL-membranes can achieve both high selectivity and permeability [4–12]. Therefore, we decided to use RTIL-membranes to determine

their potential for natural gas upgrading. In addition, their ability for CO_2 separation from permanent gases are determined.

The most important gas transport parameters of a membrane are permeability and selectivity. In this dissertation, the permeability and selectivity of main components of natural gas (CH_4, C_3H_8, CO_2, and N_2) are determined. The permeability is defined as the amount of a gas or liquid through a membrane. The permeability of a membrane is the product of gas diffusivity and solubility in RTIL. The permeability can be determined using the following formula:

$$P = S \times D \tag{1.1}$$

where P is the permeability, S is the solubility, and D is the diffusivity.

Permeability of a gas in an RTIL mainly depends on the molar volume and viscosity of the RTIL [6]. However, based on the work done by Scovazzo [6], the CO_2 permeability strongly depends on the viscosity of the RTIL. In contrast, the CO_2 permeability is not highly affected by the molar volume of the RTIL and its effect is almost negligible [6].

The selectivity of a gas pair, α_{ij}, can be determined by dividing the permeability of the faster permeating gas i with the permeability of the slower permeating gas j. The following formula is used to calculate selectivity:

$$\alpha_{ij} = \frac{P_i}{P_j} \tag{1.2}$$

where P_i and P_j are the permeability of the fast and slow permeable gases.

Since the gas transport through the RTIL-membranes is dominated by the solubility [13–17] instead of gas diffusivity, the selectivity of the RTIL-membranes mainly depends on the gas

solubility. The gas solubility in the RTILs is investigated by several researchers [18–21]. Regular solution theory was used to explain CO_2 solubility in the RTILs. According to the regular solution theory, the CO_2 solubility in the RTILs or Henry's Law Constants can be determined using solubility parameters. The following equation relates the Henry's Law Constant to the solubility parameter [16,22]:

$$Ln\left(H_{2,1}(atm)\right) = a + b(\delta_1 - \delta_2)^2 \qquad (1.3)$$

where $H_{2,1}(atm)$ is the Henry's constant in which 1 is RTIL and 2 is CO_2, δ is the solubility parameter, and a and b are empirically determined constants for a specific temperature and pressure. The solubility parameter is calculated from the following formula [16,19,22,23]:

$$\delta = \left(2.56 \times 10^6 \left(\frac{J}{mol}\right) \left(\frac{z_1 z_2 \left(\frac{cm^3}{mol}\right)^{\frac{1}{3}}}{V_{RTIL}^{\frac{4}{3}}} \right) \left(1 - \frac{0.367 \left(\frac{cm^3}{mol}\right)^{1/3}}{V_{RTIL}^{1/3}} \right) \right)^{1/2} \qquad (1.4)$$

where V_{RTIL} is the RTIL molar volume and z_1 and z_2 are the cation and anion charges, respectively.

The equation 1.4 shows that the CO_2 solubility in the RTIL depends only on the molar volume of the RTIL. This is confirmed by Scovazzo [6] using the experimental data analysis.

The CH_4 and N_2 solubility in the RTILs depends on the polarity of the RTILs [3,21]. The polarity of an RTIL can be determined using hydrogen bond accepting ability of the RTIL. The higher the hydrogen bond accepting ability which is an indication of the polarity, the more deviation from the ideal solution behavior [3,21]. Khakpay and Scovazzo showed [3] that the permeability of the CH_4 and N_2 depends linearly on the polarity in which an increase in the polarity leads to a decrease in the CH_4 and N_2 permeability. In addition, they showed that [emim][SCN]

showed the best performance for the reverse-selective separations as well as low permeability for the CH_4 and N_2. Also, [emim][SCN] can dissolve cellulose acetate [24]. Therefore, in this work [emim][SCN] has been selected to study.

In Chapter 2, the biphasic membranes are studied experimentally. The biphasic membranes are investigated to resolve the drawbacks of the supported ionic liquid membranes (SILMs). The biphasic membranes exhibit both high permeability and selectivity similar to those for RTIL-membranes. The main advantage of the biphasic membranes is that theywithstand higher cross-membrane pressures when compared to SILMs. The gas transport properties are determined for CO_2, N_2, CH_4, and C_3H_8 to test the prepared membranes' ability for the separation of CO_2 and high value hydrocarbons such as C_3H_8 from CH_4. The results confirm a satisfactory separation factor for the natural gas upgrading.

In addition to the RTIL-membranes, other materials such as carbon/carbon composite membranes are considered. However, the expected outcome was not achieved for those membrane. RTIL/graphene-hybrid might help, but it would be premature to combine before we understand gas transport/adsorption in graphene. So we looked at gas transport/adsorption in the graphene materials for this purpose. Nanoporous graphene (NPG) and graphene oxide (NPGO) membranes were selected to computationally study the CO_2 separation from methane.

In Chapter 3, NPG and NPGO films are computationally studied to examine their ability for CO_2 removal from CH_4. NPG and NPGO films are selected for CO_2 separation from CH_4 due to their surface ability to adsorb CO_2. Oxygenated functional groups are used to modify the surface of NPG films to increase the adsorption of CO_2. The results showed that the studied films are good

as adsorbents rather than membranes and NPG or NPGO are suitable for the separation of CH_4 from CO_2.

Chapter 4 includes the conclusions of the dissertation and in Chapter 5, some suggestions for the future work are given.

CHAPTER II

BIPHASIC CELLULOSE ACETATE /IONIC LIQUID MEMBRANES FOR GAS SEPARATION

In this chapter, the use of biphasic membranes for gas separation applications is investigated. We studied three types of membranes including dope, cast biphasic, and SILM membranes. The main objective was to determine the performance of cast biphasic RTIL-membranes compared to the widely studied doped and SILM membranes. This study includes CO_2 and N_2 separation from CH_4 along with the reverse-selective potential of these membranes.

2.1. Abstract

In this work, the biphasic polymer/room-temperature ionic liquid (RTIL) membranes for gas separation is investigated to overcome drawbacks of supported ionic membranes (SILMs). For this purpose, single and biphasic cellulose acetate (CA)/[emim][SCN] membranes were fabricated using the solution casting and solution casting/phase inversion methods, respectively. Infrared spectra and atomic force micrographs were generated to characterize the fabricated membranes. Moreover, the transport properties of CO_2, N_2, CH_4, and C_3H_8 gases through the CA/[emim][SCN] dope membrane (single phase), cast biphasic CA/[emim][SCN] membrane, and supported [emim][SCN] membrane were determined using a batch gas permeance system and a continuous

flow instrument. The results indicate that the supported ionic membrane (SILM) has the highest and the dope membrane has the lowest permeability for C_3H_8. On the other hand, the dope membrane has the highest permeability for N_2 and CH_4, while the cast biphasic membrane and SILM give almost similar permeabilities for these gases. The separation performance of the cast membrane is approximately similar to the SILM separation performance. The stability of the dope, biphasic, and SILM membranes are further determined, indicating there is a breakthrough point for all membranes. This point for the biphasic and SILM membranes corresponds to a similar pressure. This shows that biphasic membranes have potential to compete with SILMs for gas separation applications by improving casting procedure. The dope membrane is less stable at high pressures than the biphasic and SILM membranes, since it is in liquid state.

2.2. Introduction

Membrane technology has emerged as a viable technology for gas separation due to the advantages over other technologies of lower energy consumption, higher reliability, ease of maintenance, and lower initial cost requirements [25–28]. Membranes are used for carbon dioxide (CO_2) removal from natural gas and they are becoming competitive to the traditional methods such as amine absorption, cryogenic distillation, and pressure swing adsorption [27,29,30]. Methane (CH_4) is the main component of the natural gas, but natural gas also contains ethane, propane, and butane [28,31–33]. The processing of natural gas includes removal and capture of light hydrocarbons that are important for the downstream petrochemical units [34,35]. For achieving this separation, larger molecules should permeate faster than smaller molecules due to larger molecular size of propane and butane compared to methane; this is the reverse behavior of conventional membranes. Such membranes are known as reverse-selective membranes. RTIL-membranes have potential for

reverse-selectivity due to gas transport mechanism in the RTIL-membranes. The gas solubility in the RTIL dominates gas transport through the RTIL-membranes. Therefore, RTIL-membranes can separate larger molecules based on the gas solubility. The prime indicator of reverse-selective membranes is C_3H_8/N_2 separation [36]. Also, C_3H_8/CH_4 separation can be used as indicators of reverse-selectivity. Recently, many researchers tried to determine gas separation properties of membranes for separation of light gases; such as, H_2, O_2, N_2, CH_4, CO_2, or vapor recovery from gas mixtures [37,38].

Despite the different types of materials used to synthesize membranes, polymeric membranes are widely used for gas separation applications [29]. However, the major drawback for the polymeric membranes is that they suffer from a tradeoff between permeability and separation performance [39]. Membranes with high gas permeability generally have low separation factor, while membranes with an acceptable separation selectivity are low in the gas permeability. Cellulose acetate (CA) has been used to fabricate membranes since Loeb and Sourirajan [40] fabricated the first CA reverse osmosis membranes through phase inversion. Different methods are used to form membranes using phase inversion process including dry phase, wet phase, and dry/wet phase inversion [41]. The interactions between polymers and solvents during phase inversion has a large impact on the membrane properties [42–45]. However, in general, only traditional organic solvents have been explored [43–45]. Many researchers fabricated different CA membranes for gas separation and water purification applications [24,32,46–51].

Room temperature ionic liquids (RTIL) are salts that are liquid at room temperature [14]. RTILs have drawn great attention in recent years for the fabrication of novel and effective materials for special tasks such as CO_2 capture [52]. RTILs are environmentally friendly solvents when compared to the organic solvents. RTILs have special properties such as negligible vapor

pressure, chemical and thermal stability, recyclability, and non-flammability [51]. Many investigations have shown that CO_2 is highly soluble in most RTILs when expressed in mole/mole units [5]. The integration of ionic liquids and membranes is predicted to play an important role in providing cost-effective and energy efficient gas separation technologies to replace traditional methods [53]. SILMs are porous membranes in which ionic liquid is immobilized inside the pores of a polymeric or inorganic support by impregnating RTIL in the support [54–56].

The synthesis of an RTIL with competitive selectivity would remain only a laboratory success story unless a means to easily and continuously cast RTILs onto a membrane is found. The lack of viable casting technique for large scale industrial fabrication is a hindrance to industrial deployment of the RTIL-membranes. SILMs have shown a good performance for the gas separation. However, the major drawback is they cannot withstand over 4 bars of cross-membrane pressures which a cross-membrane pressure over 15 bars is necessary for the industrial purposes. Researchers have tried to use polymerized ionic liquid membranes and their composites with RTILs to overcome this problem [57–60]. However, the results were unsatisfactory due to low permeability and selectivity when compared to the SILMs. Another issue with SILMs, which should be addressed is the quantity of trapped RTIL, within the porous support. To resolve the later issue, the RTIL composite membranes are proposed. RTIL composite membranes are mostly polymerized ionic liquid membranes in combination with RTILs at different concentrations. The results showed the high loadings of RTIL have demonstrated improved membrane performance [61–63].

The main objective of this work is to increase the membrane ability to withstand high cross membrane pressure and RTIL loading capacity; therefore, a biphasic membrane on a polymeric support is proposed. We started by looking at the fundamental science to create a casting solution

that would result in a biphasic polymer/RTIL thin film after exposure to a polar solvent such as water. In this work, CA and 1-ethyl-3-methylimidazolium thiocyanate ([emim][SCN]) RTIL are used to cast a thin layer of CA/[eimm][SCN] biphasic film using a phase inversion method on a polytetrafluoroethylene (PTFE) support. [emim][SCN] is entrapped in the pores of CA phase. We hypothesize that the resulting membrane will have both high RTIL content and higher mechanical stability when compared to SILMs. In addition, the reverse-selective behavior of cast membranes is examined. Reverse-selective are defined as membranes in which larger molecules pass membrane faster than small molecules. This can be achieved by using RTIL-membranes. The gas transport through the RTIL-membranes is dominated by the gas solubility and gas separation is achieved by solubility instead of diffusivity. To the best of our knowledge, the gas transport properties for biphasic membranes using CA/RTIL as well as their reverse-selective behavior for gas separation applications has not been previously published. In order to achieve these goals, we determined and compared the gas permeabilities of CO_2, N_2, CH_4, and C_3H_8 using three types of membranes CA/RTIL biphasic membrane, CA/RTIL dope, and SILM to evaluate the selectivity of the following separations: CO_2/N_2, CO_2/CH_4, C_3H_8/N_2, and C_3H_8/CH_4. Furthermore, the stability of the membranes for different feed pressures are determined. These studies were done in both a single gas permeate testing unit and in tests using continuous mixed gas feeds. Since the continuous flow system does not have sensors to determine propane concentration, the batch system used to investigate the reverse-selectivity of the membranes and continuous flow instrument used to investigate CO_2/CH_4 separation.

2.3. Hypothesis

The purpose herein is to develop a casting solution and procedure that will produce a membrane film with pure RTIL trapped and surrounded by a continuous polymer phase. Figure 2.1 shows the expected biphasic membrane cross section morphology. This cast biphasic membrane will resemble SILMs in that SILMs also contain pure RTILs trapped in interconnect pores running through the polymer. The main difference of biphasic and SILM membranes is the RTIL drops are trapped in a continuous phase of polymer and the drops are not interconnected, while RTIL in the SILMs is trapped in the interconnected pores of the support which is easier to displace. Doped membranes have trapped RTIL on the molecular level in the spaces between the polymer chains forming a single phase membrane with the RTIL/polymer homogeneous phase containing a percentage of RTILs.

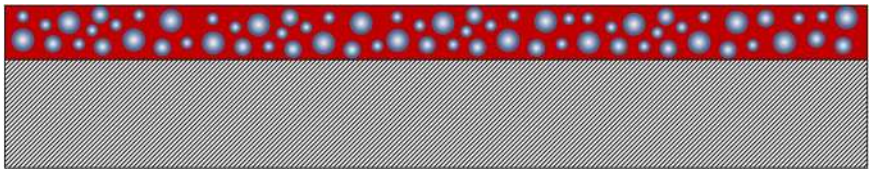

Figure 2. 1. Expected morphology of the biphasic membrane.

For our study we selected comparing our cast biphasic membrane with representatives of the prior RTIL membranes in the literature (SILMs and doped-membranes).

2.4. Experimental

2.4.1. Materials

We determined pure gas permeabilities through CA/RTIL biphasic, CA/RTIL dope, and SILM membranes. 1-ethyl-3-methylimidazolium thiocyanate ([emim][SCN], purity > 99.0%, CAS 331717-63-6, viscosity=20.79 cP, molar volume=1.52×10^{-4} m^3/mol, MW=169.25 gr/mol, hydrogen bond accepting ability=0.71 [64]) was purchased from *IOLITEC Inc.* (Tuscaloosa, Alabama). [emim][SCN] is chosen due to its high polarity (hydrogen bond accepting ability which is an indication of reduced CH_4 solubility in the RTILs [21]). In addition, [emim][SCN]'s viscosity makes it more feasible to cast flat and uniform membrane sheets. This RTIL is chosen due to its low viscosity and high hydrogen bond accepting ability which results in a low CH_4 and N_2 permeances [3,21]. Cellulose acetate (CA, purity > 97.0%, acetyl content=39.7 wt.%, CAS 9004-35-7, average Mn=50000 by GPC) was acquired from *Sigma-Aldrich*. The chemical structure of [emim][SCN] and CA is shown in Figure 2.2. Isopropanol (IP, purity > 99.5%, CAS 67-63-0) is purchased from *Fisher Scientific*.

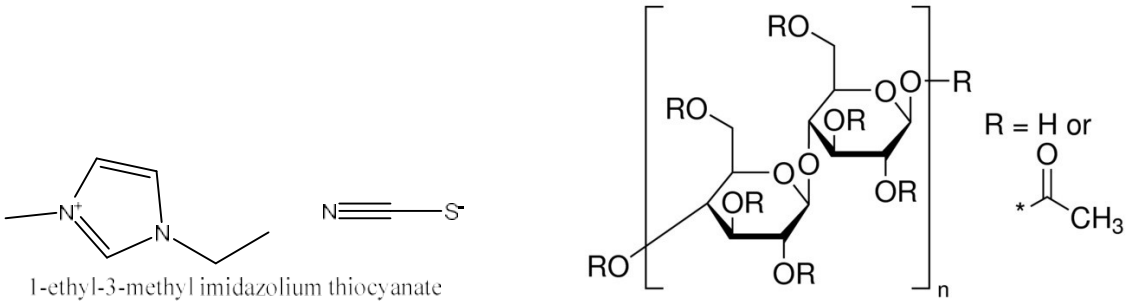

(a) *(b)*

Figure 2. 2. Chemical structures of a) [emim][SCN] and b) CA [65]

Ultrahigh purity carbon dioxide (CO_2), nitrogen (N_2), and methane (CH_4) were purchased from *NexAir* (Memphis, Tennessee). Also, propane (C_3H_8) (purity > 99.70%) was obtained from *Conley Gas* (LA Porte, Texas). The porous hydrophilic polyvinylidene fluoride (PVDF, diameter=47 mm, porosity=70%, thickness=125 μm, nominal pore size=0.1 μm, obtained from *Pall Corporation*), used for the SILM-membrane fabrications, was obtained from Millipore Corporation. The porous hydrophobic polytetrafluoroethylene (PTFE, diameter=47 mm, thickness=178 μm, nominal pore size=0.5 μm, obtained from *Pall Corporation*) was used for a backing for the biphasic and doped membranes.

2.4.2. Apparatus

The experiments were carried out in using two devices: a diffusion cell (Figure 2.3) and a continuous flow instrument (Figure 2.4). A complete description of the experimental apparatuses can be found in Morgan et al., Scovazzo et al., and Khakpay and Scovazzo [3,66,67], the following is a brief summary.

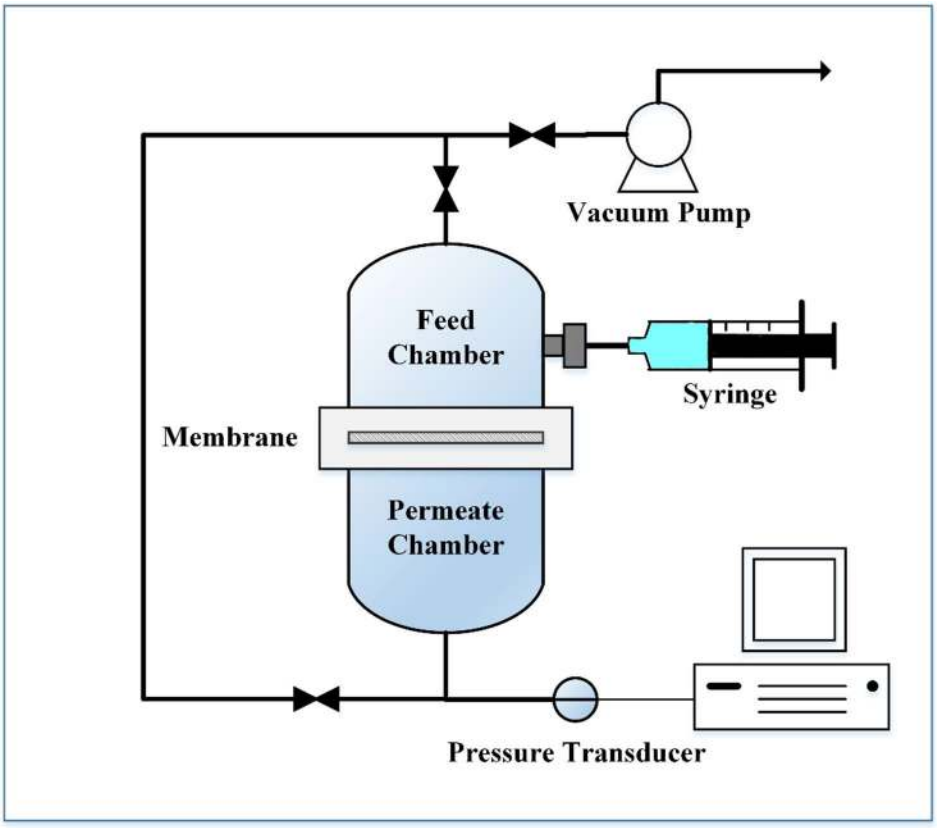

Figure 2. 3. Schematic diagram of the diffusion cell instrument for single gas permeability test [66]

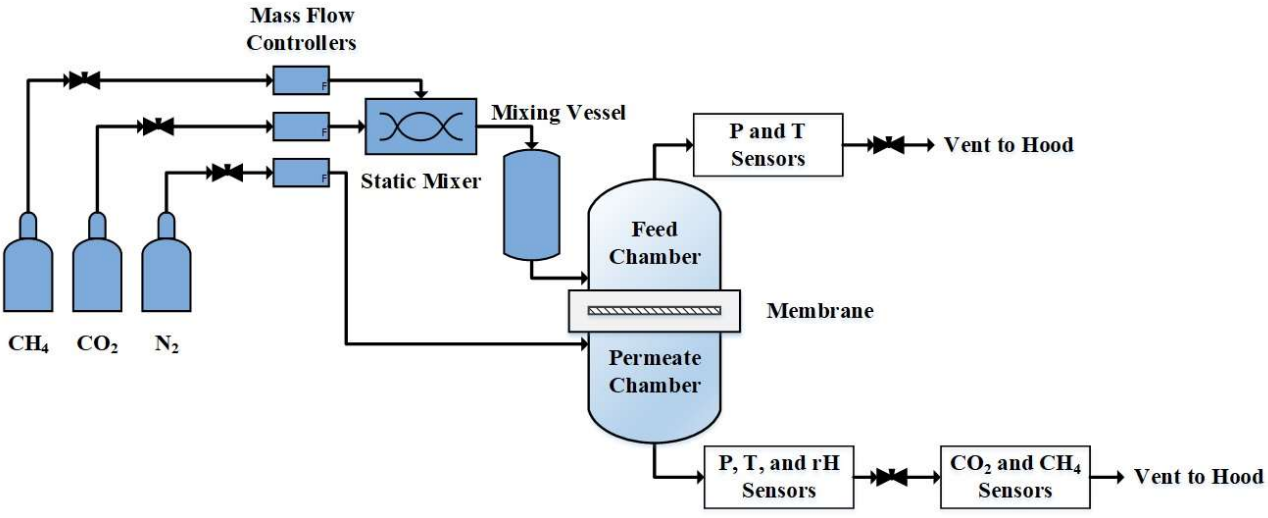

Figure 2. 4. Schematic diagram of the continuous flow instrument for mixed-gas feed permeability test

All of the single gas permeabilities are determined using the diffusion cell. The diffusion cell contains two stainless steel chambers as feed and permeate chambers. In addition, this experimental apparatus includes a vacuum pump (Fisher Scientific Maxima C Plus, Model M8C with an ultimate pressure rating of 10^{-4} Torr), a 0-5-psia pressure transducer (Omega PX811-005AV), and a PC for recording data. Furthermore, a temperature controller was used to control the unit temperature which is in an insulated box. Moreover, the unit has a septum port to inject test gases to the feed chamber using a syringe. In this work, two Viton O-rings were used to hold vacuum. The volume of feed and permeate chambers were 97 and 81 mL, respectively. The active area of the membrane was 11.064 cm^2.

The continuous flow instrument was used to determine mixed gas permeabilities for a mixed-gas feed containing CO_2 and CH_4. The continuous flow instrument was installed in a box in order to insulate it from the environment to control and keep the temperature at 30^oC. The flow rates of individual gases (CO_2, CH_4, and N_2 as sweep gas) were controlled using MKS Type 1179A Mass-Flo® controllers (MFCs) operating on a molar basis. To set gas flow rates on a desired value or a desired CO_2/CH_4 ratio instantly, the molar flow controllers connected to a MKS Type 247D Four-Channel Readout. As shown in Figure 2.3, after the flow controllers the feed stream flows into an Omega® FMX8400 Series static mixer to completely mix the gases (CH_4 and CO_2). To achieve a stabilized and thermostated mix, the mixed gas enters a Swagelok 300ml vessel (Swagelok 304L-HDF4-300). The mixed-gas leave the 300ml vessel and flows into the membrane unit which contains a stainless steel dual-chamber. The membrane unit was sealed from the atmosphere using two O-rings. The well-mixed conditions on the both sides of membrane in the membrane unit were achieved by impingement flow onto the center of the membrane support in

the both retentate and permeate side of the membrane. The active area of the membrane for the continuous flow instrument was 9.621 cm^2.

The continuous flow instrument has sensors to determine upstream and downstream conditions. The upstream sensors determined the feed condition such as temperature, and pressure. The downstream sensors measured the same properties for the retentate and permeate streams. The humidity of the retentate stream is determined to ensure that the system processed dry gases. Furthermore, the concentration of CO_2 and CH_4 were measured by means of infrared gas sensors on the permeate flow. The CO_2 and CH_4 concentrations were obtained using Vaisala GMM 221 (0–5% by volume) and Edinburgh Instruments iRcel 2179 (0–5% by volume) sensors, respectively. The accuracy and performance of both sensors were checked by using calibration gases and gas chromatographic analysis. The results are recorded spontaneously using a PC. The recorded data includes the atmospheric, retentate, and permeate pressures, box, retentate, and permeate temperatures, retentate relative humidity, CO_2 and CH_4 concentrations.

2.4.3. Methods

2.4.3.1. [emim][SCN]/CA Solution Preparation and Characterization

First, CA powder was dried at 50ºC in a vacuum oven overnight to remove the moisture. [emim][SCN] was dehydrated using a vacuum rotary evaporator. Then, CA was dissolved in [emim][SCN] with a concentration of 12 wt.%. To prevent polymer agglomeration, CA powder was slowly dispersed in [emim][SCN] while stirring [41,42]. Then, the prepared solution was

stirred for 2 days at 60ºC until CA was fully dissolved. Before using the solution, it was kept in a vacuum oven at 60ºC for 2 days to degas.

Infrared spectra were recorded using an attenuated total reflectance Fourier transform infrared spectroscopy (ATR-FTIR) (Cary 630 FTIR spectrometer, Agilent Technologies, Inc., CA, USA) with a scanning resolution of 4 cm^{-1}. The samples were analyzed over the range of 500-4000 cm^{-1} in the attenuated total reflectance (ATR) mode. Each sample was scanned at least 3 times. The morphology of the cast membrane was analyzed by an atomic force microscope (MultiMode 8, Bruker Nano, Inc.) in tapping mode.

2.4.3.2. Membrane Fabrication

The developed casting procedure used water or isopropanol (IP) as casting agents to create a biphasic membrane film. Casting membranes using isopropanol was unsuccessful due to cellulose acetate (CA) agglomeration. Therefore, we used water to prepare the biphasic membranes.

The dope and biphasic membranes were fabricated by casting [emim][SCN]/CA solution using a casting knife on a horizontal glass plate. The dope membrane was cast on layer of PTFE since the [emim][SCN]/CA solution is in the liquid state. The cast membranes are uniform and flat with a thickness of 100 μm. In order to make biphasic membrane, the prepared membrane together with the glass plate were soaked into a water or IP bath for 10 minutes to cause phase inversion of the ionic liquid/polymer solution. The resulting membrane was peeled off the glass plate. The result was a structurally stable asymmetric membrane with a PTFE backing sheet. The prepared membranes were degassed and dehydrated overnight using a desiccator under vacuum. After

completion of drying, membranes were cut in accordance with the diffusion cell and continuous flow instrument sizes. All processes were carried out at room temperature 25±1ºC.

The SILM was prepared by impregnating a porous polymer support with 1 mL of RTIL to immobilize the RTIL in the pores of the support. The polymer used for the porous stabilizing-support was hydrophilic polyvinylidene fluoride (PVDF). The fluoride backbone of PVDF is stable in the presence of [emim][SCN] and hydrophilic porous PVDF has been used before for SILMs [67,68]. The first step in fabricating the SILM is to spread 0.5 ml of the RTIL onto a watch glass using a syringe. Then, the PVDF support was placed on it to absorb the RTIL. To minimize the trapped air in the backing of the active layer of the PVDF support, the active side was placed on top of the liquid. Upon completion of the membrane wetting, the remaining 0.5 mL of the RTIL was spread over the PVDF support until it was completely soaked with the RTIL. The prepared membrane was degassed and dehydrated by a vacuum desiccator overnight, after which, the excess of the RTIL was removed from the surfaces of the membrane using a filter paper before mounting in the apparatus.

2.4.3.3. Mounting and Testing Prepared Membrane into Diffusion Cell

Since the prepared dope membrane is in the liquid state, to avoid liquid displacement and creation of pin holes due to the pressure of O-ring and feed chamber, a layer of PTFE was placed on top of the cast doped membrane. Moreover, to avoid the displacement of liquid from supporting membrane pores under pressure, a layer of porous hydrophobic polytetrafluoroethylene (PTFE) was placed beneath the prepared membrane before mounting it inside the cell. The hydrophobic nature of the PTFE support prevents its wetting with the RTIL.

The feed and permeate chambers were cleaned using ethanol and tissue papers after removing an old membrane from the apparatus. After cleaning the diffusion cell, the newly prepared membrane was installed inside the cell and the system was kept under vacuum (< 4 Pa) overnight to degas the membrane, feed and permeate chambers at 30^{o}C.

The test begins with the injection of 30 ml of the test gas onto the feed chamber. A pressure transducer continuously measured the pressure in the permeate chamber for 5 hours. The feed and permeate chambers were degassed for 1 hour after each experiment to remove the remaining gases in the membrane, feed and permeate chambers. A new experiment was started by injecting a new gas volume into the feed chamber. All experiments were repeated at least three times to ensure statistical accuracy and relevance.

2.4.3.4. Mounting and Testing Prepared Membrane into Continuous Flow Instrument

The stabilization processes for the membranes used in the continuous flow instrument are similar to the ones explained in the previous section for the diffusion cell. The feed and permeate chambers were cleaned using ethanol and tissue papers after removing old membrane from the apparatus. After cleaning the feed and permeate chambers, the newly prepared membrane was installed inside the membrane unit. Then, the mixed-gas feed flowed into the membrane unit. CH_4 and CO_2 with a ratio of 4:1 were used as feed for the mixed-gas permeability tests. The flow rates of CH_4 and CO_2 were 80 and 20 sccm (standard cubic centimeters per minute) which is close to the raw natural gas concentration for CH_4 and CO_2, respectively. Furthermore, N_2 with the flow rate of 8 sccm was used as sweep gas. The sweep gas flows directly into the permeate side of the continuous

instrument to flush the permeated gases out of the membrane unit into the sampling sensors. Having reached steady-state condition, which is about 2 hours for each experimental change in the feed condition, the data was collected for 1 hour and averaged before analysis. A new experiment was started by a change in the feed pressure. All experiments were repeated at least three times to examine the repeatability of results.

2.5. Data Analysis

To determine the permeability in the batch system, the slope of the pressure as a function of time curve in the pseudo-steady state range of data was used.

The permeability and selectivity of the gases in the continuous flow instrument are determined under the assumption that the gases in the feed and permeate are well-mixed [67]. The following formula can be used to calculate the selectivity [67] under these well-mixed conditions:

$$\alpha_{ij} = \frac{x_{p.i}}{x_{p.j}} \left[\frac{\left[(1 - x_{r.i}) - \left(\frac{P_p}{P_r} \right) x_{p.j} \right]}{x_{r.i} - \left(\frac{P_p}{P_r} \right) x_{p.i}} \right] \tag{2.1}$$

where α is the selectivity, i is the fast permeable gas, j is the slow permeable gas, $x_{r.i}$ is the mole fraction of the gas i in the retentate stream, $x_{r.i}$ is the mole fraction of the gas j in the retentate stream, $x_{p.i}$ is the mole fraction of the gas i in the permeate stream, $x_{p.j}$ is the mole fraction of the gas j in the permeate stream, P_r is the retentate stream pressure, and P_p is the permeate stream pressure.

To check the calculation results, selectivities were also calculated using gas permeances. Gas permeance was calculated using the sweep gas flow rate combined with the fluxing species mole fractions in the feed and permeate streams. The feed and permeate gas mole fractions were determined by gas analysis. The following equation calculated fluxing gas flow rate [67]:

$$G_i = \frac{x_{p.i}}{x_{p.Sweep}} G_{Sweep} \tag{2.2}$$

where G_i is the gas i flow rate, $x_{p.Sweep}$ is the mole fraction of sweep gas in the permeate stream, and G_{Sweep} is the sweep gas flow rate. The gas permeance can be calculated using the gas flow rate, gas driving force, and membrane active area. Therefore, the gas permeance is calculated using following equation [67]:

$$L_i = \frac{G_i}{A\left(P_r x_{r.i} - P_p x_{p.i}\right)} \tag{2.3}$$

where L_i is the gas i permeance and A is the membrane active area. Then, the selectivity can be determined by dividing the permeance of fast permeable gases to the permeance of slow permeable gas.

2.6. Results and Discussion

2.6.1. Membrane Characterization

Figure 2.5 shows the FTIR spectra for the pure [emim][SCN], doped, and biphasic membranes. The peaks for the wavenumbers less than 1600 cm^{-1} is mainly due to the presence of imidazolium

ring. Furthermore, the peak at 2050 cm^{-1} shows the -C≡N stretching of the anion. Similar results are published in the previous studies [42,69,70].

The hydrogen bonding between the [emim] cation and [SCN] anion in the pure [emim][SCN] is confirmed by the presence of broad bonds in =C-H stretching region around 3120 cm^{-1} and –C-H stretching close to 3020 cm^{-1}. Chung et al. [42] and Dupont [71] reported similar results for the pure [emim][SCN]. The experimental and computational studies confirmed that imidazolium based RTILs have a charge-ordered structure because of their Coulombic interactions and hydrogen bonding between ions of RTIL [42,71–74]. This expedites the self-organization of the RTILs [42,71–74]. In addition, Figure 2.5 shows that the addition of 12 wt% of CA to the [emim][SCN] does not shift the wavenumbers of hydrogen bonded C-H group. Moreover, similar results are determined for the cast membrane. This indicates that the CA chains are enclosed by the cations and anions of the RTIL indicating that the network of RTIL ions are still continuous and remains at a good extent. Furthermore, the addition of the CA to the RTIL does not break the RTIL network and it is still continuous showing that RTIL structure does not change in the CA and [emim][SCN] mixture because of the strong hydrogen bonding and Coulombic forces for both dope and cast membranes. Similar results are reported by Chung et al. [42].

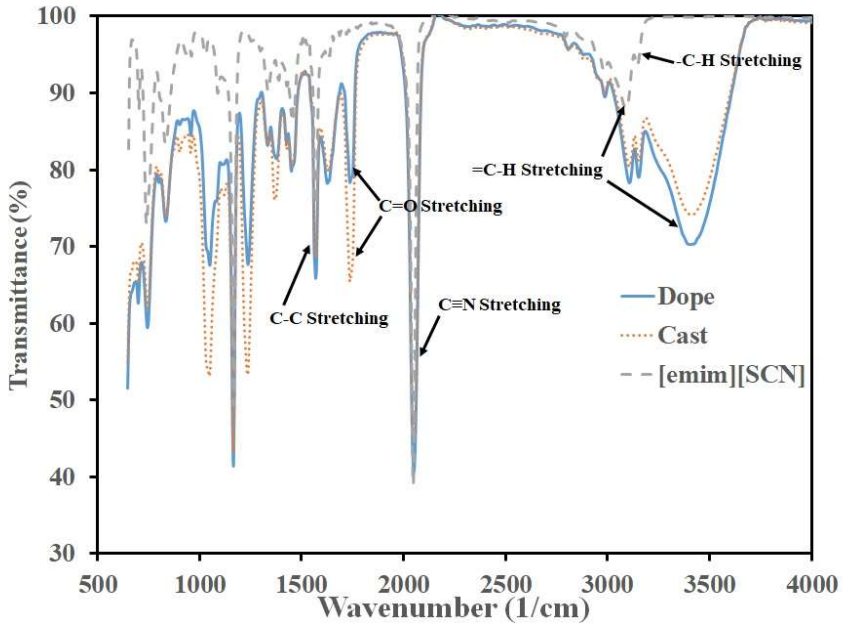

Figure 2. 5. The FTIR spectra for pure [emim][SCN], dope, and cast biphasic membrane

In addition to the FTIR tests, images from the surface of the cast biphasic membrane were taken using AFM. The results are shown in Figure 2.6. The results show that the membrane surface is a combination of CA agglomerated regions and uniform region (see Figure 2.6). The presence of agglomerated CA is due to the phase separation into the RTIL rich and CA rich phases which is due to miscibility of the [emim][SCN] in the water. This image indicates that the cast biphasic membrane is mainly uniform showing the satisfactory casting procedure. Furthermore, the phase image confirms the presence of CA agglomerated regions (white regions in Figure 2.6).

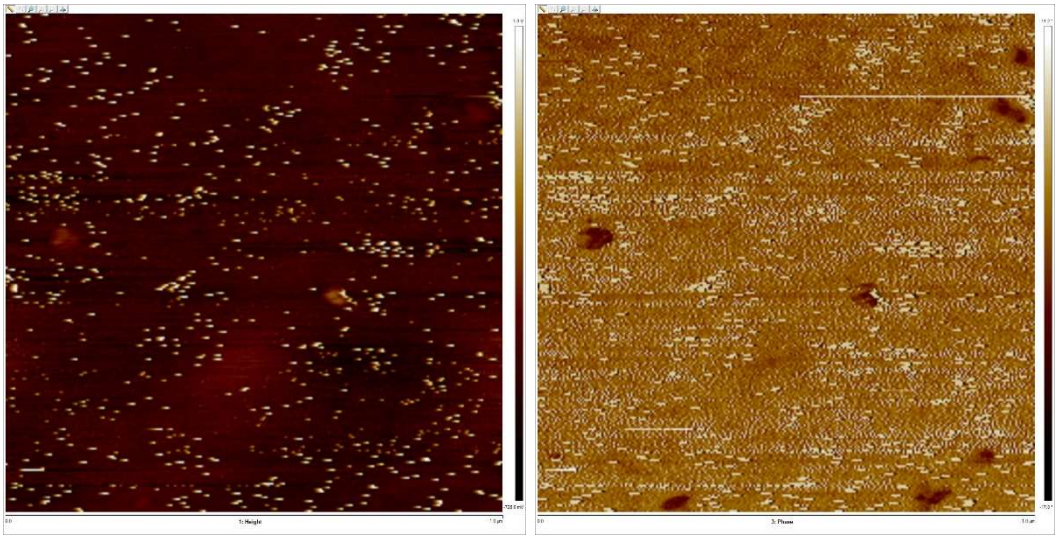

(a) *(b)*

Figure 2. 6. AFM images of cast membrane: a) surface topography b) phase distribution.

The white regions are CA rich regions while, the brown regions are RTIL rich regions.

2.6.2. Permeability Results

Gases penetrate through the dope, biphasic, and SILM membranes with different mechanisms. The gas transport mechanism through the dope membranes is a solution-diffusion mechanism. Therefore, the permeability of gases can be determined directly using equation 1.1 since the dope solution is the only available media for gas transport. Figure 2.7 shows the gas transport mechanism through the dope membrane.

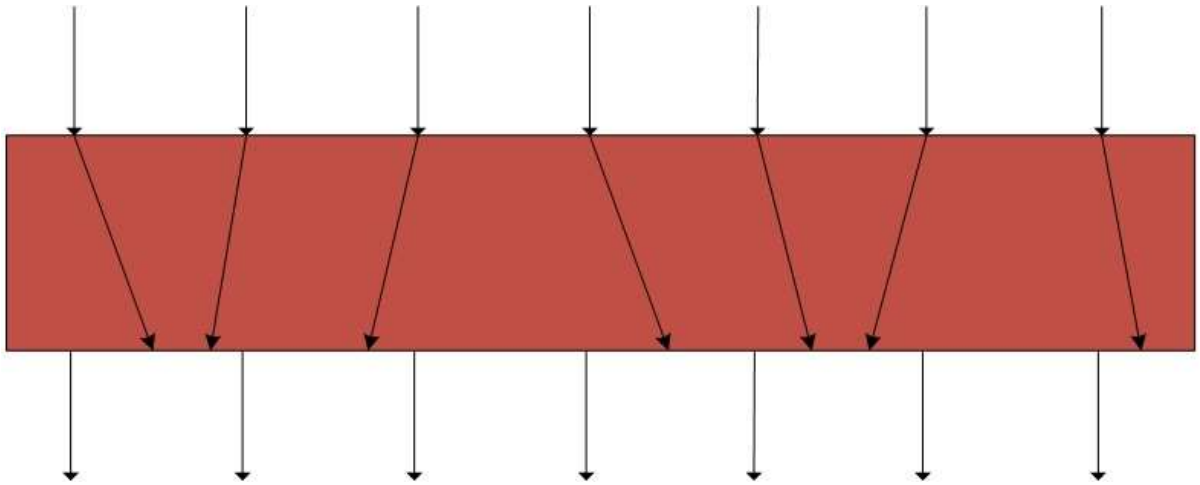

Figure 2. 7. Gas transport through the dope membrane.

Figure 2.8 shows the gas transport mechanism through the biphasic membrane. Similar to the dope membrane, gas transport mechanism through the is a solution-diffusion mechanism. However, the available media for the gas transport through the biphasic membrane is different. The gas molecules pass through the continuous polymer bulk and RTIL pockets in the polymer bulk. First, gas molecules diffuse through the polymer surface. Some gas molecules pass the biphasic membrane without passing the RTIL pockets. Since the gas diffusion coefficient in solids is smaller when compared to those in liquids, the permeation through the polymer bulk is slow. However, after diffusion through the biphasic membrane surface, some gas molecules reach to the RTIL pockets in the polymer bulk. The gas transport in the RTIL pockets is dominated by the solubility. Therefore, gas transport through the RTIL pockets are fast when compared to that of polymer bulk. After passing through the RTIL pocket, gas molecules diffuse through the polymer bulk to reach another RTIL pocket or the other side of the biphasic membrane. The gas permeability through the biphasic membrane can be determined using the theoretical models for

the permeability through mixed matrix membranes. Maxwell model is one of the theoretical models to determine gas permeability through a mixed matrix membrane [75]:

$$P_{ra} = \frac{P_e}{P_m} = \frac{1+\frac{2\phi(\lambda_d-1)}{(\lambda_d+2)}}{1-\frac{\phi(\lambda_d-1)}{(\lambda_d+2)}} \quad (2.4)$$

where P_{ra} is the permeability ratio, P_e is the effective gas permeability in the mixed matrix membrane, P_m is the gas permeability in the matrix (continuous phase), ϕ is the volume fraction of the filer particles (the RTIL pockets), and λ_d is the permeability ratio. λ_d is calculated using following equation:

$$\lambda_d = \frac{P_d}{P_m} \quad (2.5)$$

where P_d is the gas permeability through the dispersed phase (the RTIL pockets).

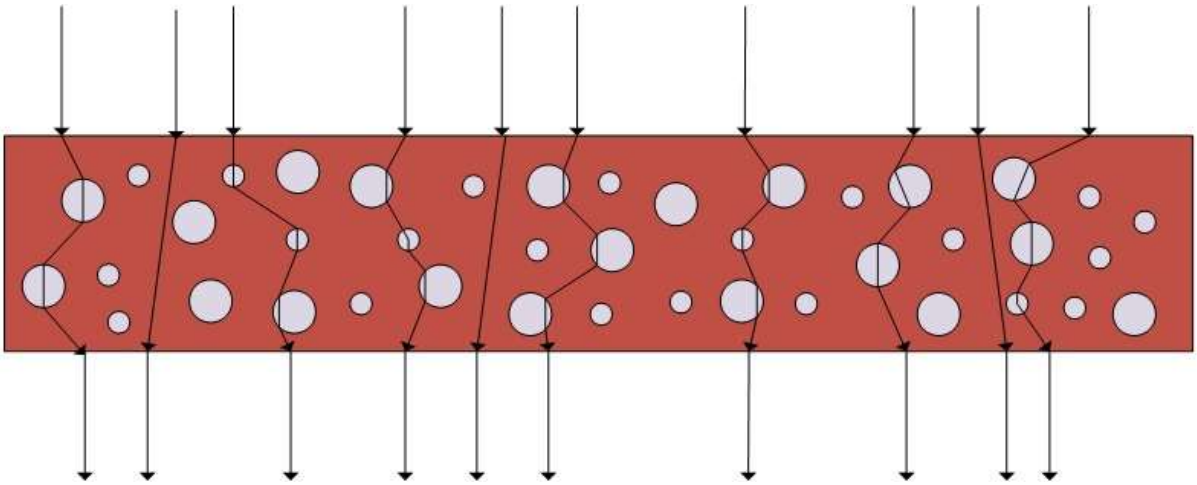

Figure 2. 8. Gas transport mechanism through the biphasic membrane.

Figure 2.9 presents the gas transport mechanism through the SILMs. Similar to the dope and biphasic membranes, the gas transport mechanism in the SILM is diffusion-solution. Gas molecules can permeate in the SILMs through the support and RTIL. The overall permeability is the summation of gas permeation through the support and RTIL. The gas permeability through the SILMs is determined using following equation:

$$P = \phi P_{RTIL} + (1 - \phi) P_{Support} \quad (2.6)$$

where P_{RTIL} and $P_{Support}$ are the gas permeabilities in RTIL and support, respectively.

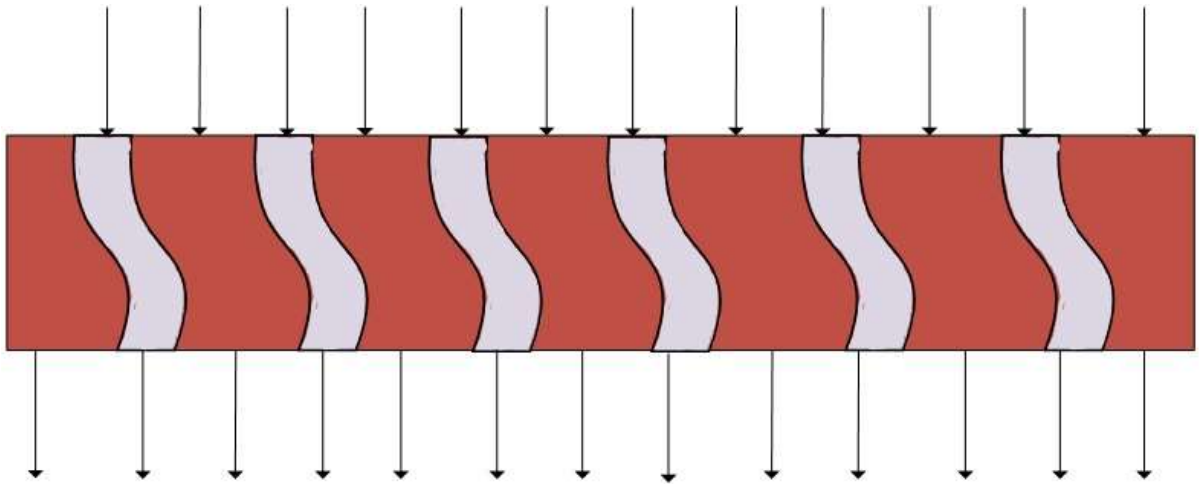

Figure 2. 9. Gas transport mechanism in SILMs.

The gas permeability through the polymeric support is negligible when compared to that of RTIL. Because, gas transport in RTILs based on the solubility. In contrast, gas diffusion through support is smaller than that of RTIL. Therefore, the gas permeability in SILMs depends only on the gas transport through RTIL. The following formula is used to determine gas permeability:

$$P = \phi P_{RTIL} \quad (2.7)$$

The reverse-selectivity of the dope, biphasic, and SILM membranes are studied using the batch instrument due to limitations of the continuous flow system for C_3H_8. The main assumption for determination of permeabilities in this experimental study is that gas separation is completely because of the prepared membrane films; the PTFE backing does not impact the gas separation. Furthermore, the determined permeabilities are affected by the leakage rate into the permeate chamber of the test equipment (Section 2.4.2) which is 1.5 Barrers (1 Barrer = 10^{-10} $cm^3_{STP}.cm/(cm^2.s.cmHg)$).

The permeabilities were determined using the steady state region of data. The pure gas permeabilities for CO_2, N_2, CH_4, and C_3H_8 were determined using initial pressures of approximately 30 kPa at 30ºC (Table 2.1). The permeability and selectivity results for the CO_2 involving separations are reported in the Appendix A, because the CO_2/CH_4 separation was studied using continuous flow system and the results are in Section 2.6.4.

The SILMs showed the highest permeability for the C_3H_8, while the biphasic membrane had the lowest permeable membrane for the C_3H_8. The permeability of N_2 are almost the same for the studied membranes. Furthermore, CH_4 is less permeable in the SILM and the biphasic membranes compared to the dope membranes. The CH_4 permeability for the SILM and biphasic membranes are approximately the same.

For the RTIL-membranes gas transport is dominated by solubility and the performance of RTIL-membranes are highly affected by the RTIL content in the membrane. The RTIL content of the dope, cast, and SILM membranes are 89, 71, and 70 v.%, respectively. Since the dope membrane has the highest RTIL content among the tested membranes, it should be the most permeable membrane for all gases because the solubility dominates gas transport through RTIL-membranes. However, only CH_4 permeate faster through the dope membrane.

The mechanism of gas solubility in RTILs is studied computationally [76,77]. The results showed that gas molecules occupy the fractional free volume of the RTILs to dissolve in RTILs. The fractional free volume in the RTIL depends inversely on the viscosity of the RTIL. Therefore, the capacity of RTIL to dissolve gas molecules deteriorates when viscosity of RTIL increases. This is in agreement with the work published by Scovazzo [6] in which an increase in the viscosity leads to a decrease in the gas permeability.

Gas transport mechanism through the dope membrane is different because of CA presence in the RTIL. The reason that gas permeabilities are lower than the expected values (higher than corresponding gas permeabilities for the biphasic and SILM membranes) can be due to the presence of CA molecules in the free volumes between the RTIL molecules. CA molecules may take the available space between RTIL molecules during the dissolving of CA in the RTIL. Therefore, the fractional free volume of the RTIL will decrease. Since the fractional free volume is the main and available path for gas transport [76–78] and this space is partially filled by the CA molecules in the dope membrane, the gas permeabilities are lower than expected values (higher than corresponding gas permeabilities for the biphasic and SILM membranes).

Table 2. 1. Experimental gas permeances in Barrers (1 Barrer = 10^{-10} $cm^3_{STP}.cm/(cm^2.s.cmHg)$) at 30°C.

Membrane	Permeability (Barrers)		
	N_2	CH_4	C_3H_8
CA/[emim][SCN]	7.6 ±0.8	19±1	40±1
Biphasic membrane	6±1	13.8±3	29±3
SILM([emim][SCN])	6±1	12±1	80±10
SILM ([emim][Tf_2N])	73.6 [a]	139.2 [a]	-
SILM ([emim][DCA])	21.8 [a]	53.8 [a]	-
Polyimide membranes	0.474 [b]	0.19 [c]	0.013 [c]

[a] All data are determined from [6].

[b] All data are determined from [79].

[c] All data are determined from [80].

To the best of our knowledge, the gas permeabilities for N_2, CH_4, and C_3H_8 through the RTIL-membranes for the [emim][SCN] have not been published yet except the work published by this group [3]. Therefore, the reported gas permeabilities in Table 2.1 from the literature are for the benchmark RTILs that define the upper-bound for RTIL-membranes. The permeabilities for the studied gases are lower when compared to those in the literature for the RTIL-membranes. One reason is the difference in the viscosity of the RTILs. The lower the viscosity of the RTIL, the higher the gas permeability. However, the permeabilities of N_2, and CH_4 are higher than the permeabilities of these gases through the polyimide membranes.

2.6.3. Selectivity Results

The ideal selectivity, α_{ij}, was determined by dividing the permeance of the faster permeating gas i with the permeance of the slower permeating gas j. Table 2.2 shows the selectivities for CO_2/N_2, CO_2/CH_4, C_3H_8/N_2, and C_3H_8/CH_4 separations at 30ºC.

Table 2. 2. Experimental gas selectivities at 30ºC.

Membrane	C_3H_8/N_2	C_3H_8/CH_4
CA/[emim][SCN]	5±2	2.1±0.6
Biphasic membrane	5±3	2.1±0.8
SILM	14±4	7±2
SILM ([emim][Tf_2N])	-	-
SILM ([emim][DCA])	-	-
Polyimide membranes	-	0.1 [a]

[a] All data are determined from [80].

The highest selectivity is observed for the SILM for all gas separation, because the SILM membrane showed lower permeances for the slow permeable gases which are N_2 and CH_4. The

separation performance of the biphasic membrane is close to the dope gas separations. The lower selectivity of the dope and biphasic membranes are because of their low permeability for the fast permeable gas (C_3H_8) and higher permeabilities for the low permeable gases (N_2 and CH_4).

SILMs showed the reverse-selectivity for the C_3H_8/N_2 and C_3H_8/CH_4 separations. In contrast, the dope and biphasic membranes selectivities for the C_3H_8/N_2 and C_3H_8/CH_4 separations are still larger than 1 however, they are smaller than those reported in the literature for the polymeric membranes. The lower selectivity of the dope and biphasic membranes than those of the SILM indicates that the casting procedure should be improved in order to make more efficient membranes. More details regarding improving casting procedure are given in Chapter 5.

Even a very small leak in the permeate chamber leads to the overestimation of the permeability of slower permeating gases such as N_2 and CH_4 especially in the RTILs. Therefore, the experimentally reported selectivity could be lower than those obtained from ideal test equipment with no leaks. For example, the lowest determined permeance is 6 Barrers for N_2 permeance in SILM which is 4 times the leakage rate. To avoid the leakage rate and to determine accurate separation factors, the gas transport properties should be determined at high pressures (> 1 bar). Therefore, the permeabilities of CO_2 and CH_4 are determined using a continuous flow instrument. Furthermore, the stability of tested membranes as a function of pressure are determined and results are presented in the next section.

2.6.4. Stability of Membranes

Due to equipment limitations of the batch system, we used the continuous flow instrument to examine the stability of the membranes at high pressures. The permeability and selectivity of CO_2

and CH_4 mixture are determined at different feed pressures. The feed ratio for the CO_2 and CH_4 mixture was 4:1 which is close to the raw natural gas concentration. The permeabilities of CO_2 and CH_4 are shown in Figures 2.10 and 2.11.

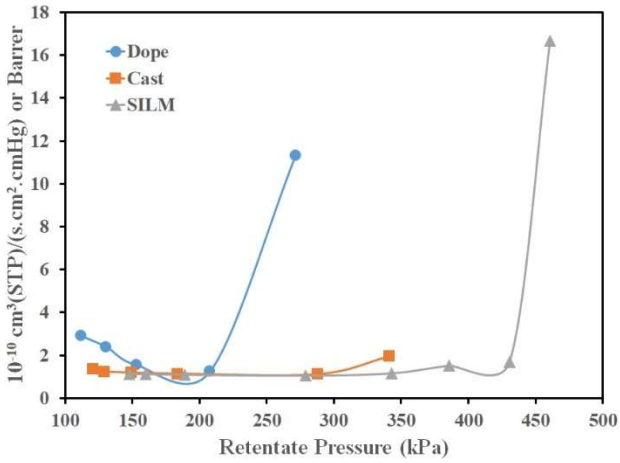

Figure 2. 10. The permeability of CO_2 as a function of retentate pressure. Initially the permeability decreases when retentate pressure increases. Then there is a drastic increase in the permeability which arises from the membrane breakthrough point.

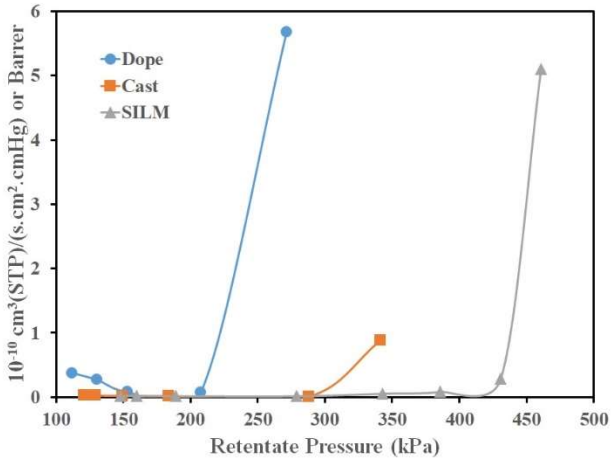

Figure 2. 11. The permeability of CH_4 as a function of retentate pressure. The permeability decreases when retentate pressure increases. Also, there is a drastic increase in the permeability which arises from the membrane breakthrough point.

The permeability of CO_2 and CH_4 decreases when retentate pressure increases. This is interesting since the higher pressure leads to the higher gas solubility in the RTIL which results in the higher permeability. This behavior can be explained by the deformation of the shape of supporting polymer. The supporting polymer deforms at high pressure in which the size of membrane pores decreases. The compression of the membrane pores leads to a decrease in the active separation area of the membrane and to an increase the tortuosity. This explanation has not been proven yet and more studies are needed to prove this. Similar results for the H_2 permeation through the SILMs are reported by Belafi-Bako et al. [81].

The permeability of CO_2 and CH_4 increases significantly after the breakthrough point. In the breakthrough point, the gas permeabilities increase considerably which is an indication of RTIL displacement in the polymeric support. The breakthrough point for the gas permeabilities through the dope membrane occurred at around 200 kPa, while the breakthrough point for the cast

biphasic and SILM membranes are around 300 and 440 kPa, respectively (Figures 2.9 and 2.10). The lower breakthrough pressure for the dope membrane can be due to the displacement of the dope solution between the PTFE layers and creation of dry regions in the membrane since it is stabilized between two layers of PTFE. For the cast biphasic and SILM membranes, the breakthrough point happens when RTILs is pushed out of the polymeric support. The capillary forces of the pores are responsible for the pores holding the RTIL. The RTIL molecules remain in the pores as long as gas pressure is low (< 2 bars). For the dope membrane is stable until the gas exerts enough force to move the dope molecules. If the capillary forces are larger than the forces required for moving the dope molecules, it would explain why the breakthrough point for the cast biphasic and SILM membranes occurred at higher pressures.

The escalation of the gas permeability as it does not affect the separation performance is preferred. Therefore, the membrane selectivity is a better tool to examine the membrane stability. The breakthrough point for a membrane can be defined as a pressure in which the separation performance drops considerably.

The selectivity of CO_2 and CH_4 separation is presented in Figure 2.12. Similar to the permeability results, there are breakthrough points for the studied membranes. The breakthrough points correspond to the similar pressure for the permeabilities. As shown in Figure 2.11, the cast biphasic membrane showed higher selectivity for the CO_2 and CH_4 separation, while the dope membrane presents the lowest selectivity. At first look, these results are in contrast with the results in the Appendix A. However, the results are in agreement when comparing the results statistically. The standard deviation for the selectivities determined using batch system are 8 and 10 for the cast and SILM, respectively indicating that the selectivity of the cast membrane can be higher than

SILM. In addition, the determined selectivities using continuous flow instrument are more reliable than diffusion cell since there is no method error resulting from a leak rate.

The higher selectivity of the cast biphasic membrane can be due to the higher RTIL content of the cast biphasic membrane when compared to the SILM membranes. Since the breakthrough point for the cast biphasic and SILM membranes is at the same pressure, the cast biphasic membrane improves only the membrane separation factor. However, future modification of the casting procedure and agent could improve both membrane separation performance and stability (see Chapter 5).

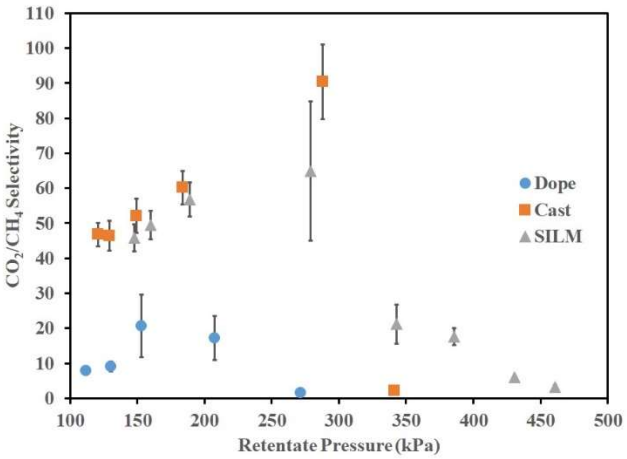

Figure 2. 12. The effect of retentate pressure on the selectivity of CO_2/CH_4 separation. The selectivity increases with an increase in the retentate pressure. However, there is a breakthrough point in which the membrane performance considerably declines.

2.7. Conclusions

In this experimental work, the potential ability of the biphasic membranes for gas separation applications are examined. Furthermore, the reverse-selective behavior of the biphasic membrane

is investigated. The biphasic membrane is fabricated using CA and [emim[SCN]. The FTIR tests and AFM imaging are done to characterize the membranes. The gas transport properties of the dope (CA/[emim][SCN]) and SILM are also obtained to assess the cast biphasic membrane performance.

The FTIR tests shows strong interactions of [emim][SCN] with CA molecules with the hydrogen bonding, Coulombic forces, and van der Waals interactions. The CA dissolving in [emim][SCN] is strongly affected by these interactions. The permeabilities of CO_2, N_2, CH_4, and C_3H_8 are determined using a diffusion cell and a continuous flow instrument. The results showed that the SILM is the most permeable membrane for CO_2 and C_3H_8, while the dope membrane was less permeable for these gases. In contrast, the dope membrane showed the highest permeability for N_2 and CH_4. The permeability of N_2 and CH_4 through the biphasic and SILM membranes were almost the same. The dope membrane showed the lowest selectivities for all of the membranes. The separation performance of the biphasic and SILM membranes were similar for the CO_2/N_2 and CO_2/CH_4 separations. The stability of the dope, biphasic, and SILM membranes as a function of retentate pressure are examined and the results showed that the biphasic and SILM membranes have the similar breakthrough point. The dope membrane was less stable when compared to the biphasic and SILM membranes. In addition, the biphasic membrane is the best for the CO_2/CH_4 separation, while SILM is a better membrane for the reverse-selective separations. The biphasic membrane show promise to resolve drawbacks of SILMs. The prepared biphasic membrane in this study showed better separation performance while it was 20% thinner.

CHAPTER III

MOLECULAR INSIGHTS ON THE CH_4/CO_2 SEPARATION IN NANOPOROUS GRAPHANE AND GRAPHENE OXIDE SEPARATION PLATFORMS: ADSORBENTS VERSUS MEMBRANES

This chapter investigates the CO_2 separation from CH_4 using nanoporous graphene (NPG) and graphene oxide (NPGO) membranes. NPG and NPGO membranes were studied as adsorbents and membranes. Molecular dynamics simulations were performed to gain fundamental molecular insights on the concentration-dependent adsorption and gas transport properties of the components in a CH_4/CO_2 gaseous mixture in single- and double-layered NPG and NPGO separation platforms. The simulation time selected to be 120 ns. This time is determined based on the steady sate point of the NPG and NPGO sheets. The simulation time to reach steady state differs the time in the real life system to reach steady state. Therefore, a time scale or factor should be defined to relate the simulation results to the experimental results. The results of this chapter are published in the Journal of Physical Chemistry C [28].

3.1. Abstract

Molecular dynamics simulations were performed to gain fundamental molecular insights on the concentration-dependent adsorption and gas transport properties of the components in a CH_4/CO_2 gaseous mixture in single- and double-layered nanoporous graphene (NPG) and graphene oxide (NPGO) separation platforms. While these platforms are promising for a variety of separation applications, much about the relevant gas separation mechanisms in these systems is still unexplored. Based on the gas adsorption results in this work, at least two layers of CO_2 are formed on the gas side of both NPG and NPGO, while no adsorption is observed for pure CH_4 on the single-layered NPG. In contrast, increasing the CH_4 concentration in the CH_4/CO_2 mixture leads to an enhancement of the CH_4 adsorption on both separation platforms. The through-the-pore diffusion coefficients of both CO_2 and CH_4 increase with an increase in the CH_4 concentration for all NPG and NPGO systems. The permeance of CO_2 is smaller than that of CH_4, suggesting the NPG and NPGO platforms are more suitable as CO_2 adsorbents or membranes for the CH_4/CO_2 (rather than the CO_2/CH_4) separation. The highest observed selectivities for the CH_4/CO_2 separation in the NPG and NPGO platforms are about 5 and 6, respectively.

3.2. Introduction

Separation of CO_2 from CH_4 is important for processes such as natural gas sweetening, biogas upgrading, and landfill gas purification [82,83]. Furthermore, CO_2 is a corrosive impurity (acid gas) in raw natural gas streams that needs to be removed [84]. Membranes, which allow for a simple and energy-efficient separation of gases, have emerged as alternatives for the traditional gas separation processes, such as solvent absorption, solid adsorption, and cryogenic distillation [85,86]. Separation in membranes is based on mechanisms such as selective component

adsorption, component diffusion rate differences, solution-diffusion, or molecular-sieving [56,87]. Organic (polymeric), inorganic, and mixed-matrix membranes are currently available for the CO_2 and CH_4 separation [88–91]. Among these, inorganic membranes are more efficient under severe operating conditions, such as high temperatures and pressures [92]; however, a major drawback for these membranes is their high production cost.

Nanoporous pristine graphene (NPG) and graphene oxide (NPGO) and their composites have shown promising performance in certain membrane [87] and gas adsorbent applications [93,94]. A graphene sheet, which is a two-dimensional (2D) sheet of sp^2-hybridized carbon, is considered a unique separation platform with desirable flux properties so long as it has a porous structure. From both theoretical and experimental perspectives, pristine graphene has been shown to be impermeable, even for small gases like helium, because of its substantial electron density of aromatic rings [95–99]. Therefore, highly selective membranes can only be obtained in porous graphene-based material systems [95,96,100–103]. The thickness of the selective membrane layer in these systems ranges from tens of nanometers to several micrometers [99,104,105].

Despite the simple structure of graphene, it is difficult to drill holes in it [95]. Nevertheless, NPGO separation platforms as membranes are getting increased attention because of their robustness, structural integrity, and ease of fabrication and scale-up [106–109]. NPGO is the chemically modified NPG with oxygenated functional groups, such as hydroxyl, carbonyl, epoxy, and carboxyl on its surface, edges, and pore rims [110]. The surface functionalization of NPG may have a positive or negative effect on the membrane separation performance [95,108]. NPGO has large surface area for storing and separating polar gas molecules [95,111]. Its porosity and available surface area can be adjusted for different applications by varying the interlayer spacing

in the layered NPG and NPGO structures or by using different surface, edge, and pore rim functional groups [95].

The gas separation performance of NPG and NPGO as membrane platforms mainly depends on their average pore size, which is typically very small. For example, Tao et al. [96] report an average pore size of 9 Å for the NPG membrane used in their work. On the basis of small pore sizes in NPG and NPGO membranes, use can be made of molecular dynamics (MD) simulation to study the pore-size-dependent separation phenomena in these systems [104], thus rendering the use of traditional continuum approaches unfeasible. Despite the technical importance of NPGs, previous MD simulation studies have only elucidated the effect of a single pore on the gas separation. There are still many aspects of gas transport through these membranes that are hitherto unexplored. In what follows a summary of previously published computational work for gas separations in graphene- or other porous carbonaceous membranes is given.

Schrier [112] carried out an MD simulation to examine the graphene surface adsorption potential for CO_2, CH_4, N_2, O_2, H_2S, SO_2, and H_2O. Graphene was found to be useful for CO_2 capture and separation. The adsorption capacity of CO_2, CH_4, and N_2 on an ordered mesoporous carbon structure at different temperatures was determined by Yuan et al. [113] Based on their simulation results, the versatile mesoporous carbon structure has a large adsorption capacity and high selectivity for the separation of CO_2, CH_4, and N_2 gases. Lu et al. [114] determined the adsorption and separation properties of CO_2 and CH_4 on pristine mesoporous carbonaceous structures, carbon foams, carbon nanotubes, and nanoporous carbon structures modified with carboxylic acid groups using MD simulation. Their results indicate that gas separation in carbon nanopores is mainly affected by the nature of the matrix and heterogeneity of the materials. Trinh et al. [115] obtained the separation properties of the CO_2/CH_4 mixture in mesoporous

carbonaceous structures by MD simulation. Based on their findings, a perfect charged graphite model gives lower values for the selectivity of the CO_2/CH_4 mixture. Moreover, a high adsorption-selectivity of 25 can be achieved with a charged defect of 0.45 electrons/atom. The adsorption capacity of CO_2 and CH_4 on mesoporous carbon and graphene has been reported in several studies [116–119], indicating that these nanoporous materials have potential to adsorb and separate CO_2 and CH_4 mixtures.

Sun et al. [120] and Jiao et al. [121] determined the diffusivity of CO_2 and CH_4 in graphene-based membranes using MD simulation. Their results indicate that the diffusion coefficient of CH_4 is higher than that of CO_2 for all membranes used in their study. Zhang et al. [122] report the CH_4 diffusivity through dry and moist coal to be 1.290×10^{-9} and 0.083×10^{-9} m^2/s, respectively. To the best of our knowledge, the work of Zhang et al. is the only published one to date in which the CH_4 diffusivity in a carbonaceous material with a structure similar to that of graphene is reported. The gas permeance through an NPG membrane was studied by Liu et al. [123] They considered several gases, including CO_2, in their study. They further modified the membrane pore rims with nitrogen molecules. The CO_2 permeance through the modified NPG membrane was found to be 2.8×10^5 GPUs (1 GPU or gas permeation unit $\approx 3.35\times10^{-10}$ mol m^{-2} Pa^{-1} s^{-1}). The CH_4 permeance through an NPG membrane for different pore sizes was determined by Sun et al. [101] They utilized MD simulation to determine the gas transport properties in this membrane. Based on their results, gas permeance depends on the membrane pore size.

One objective in this work is to elucidate the mechanisms associated with the CH_4/CO_2 separation in NPG and NPGO separation platforms using MD simulation, thereby suggesting their applicability for membrane or gas adsorbent applications. Since the effects of gas molar concentration, number of membrane/adsorbent layers, and surface chemistry (pristine versus

oxidized) on the CH_4/CO_2 separation performance of the nanoporous graphene-based material systems have not fully been investigated before, another objective in this work is to determine these effects. Moreover, the CH_4 and CO_2 adsorption and transport data, such as adsorption capacity and isotherms, diffusion coefficients, permeance, and membrane selectivity, as a function of gas molar concentration and number of membrane layers were generated and compared. This comprehensive study provides molecular insights on the performance of nanoporous graphene-based separation platforms for the CH_4/CO_2 separation, and the methodology used herein can be adopted for the fundamental investigation of other gas separations in these systems.

3.3. Computational Method

Models of porous finite hydrogen-terminated single- and double-layered NPG and NPGO sheets were created in BIOVIA Materials Studio (v8.0). Three elliptic pores (a = 10.0 Å, b = 12.3 Å) were introduced in each layer of both systems, as shown in Figures 3.1a and 3.1b. In the NPGO sheets, the graphene layer was functionalized with hydroxyl (-OH) and/or epoxide (-O-) groups on the surface and pore rims and with carboxylic acid (-COOH) groups on the edges (Figure 3.1b) [124,125]. Next, a single NPG or NPGO sheet was placed in the middle of a 2D-periodic simulation cell (periodicity in the x- and y-directions) with the average size of 47×43×100 $Å^3$. Similar systems were created for two stacked NPG (designated as 2NPG) or two stacked NPGO (2NPGO) sheets, which were placed 12.4 Å apart, with the second layer rotated 180º in plane, in a 2D-periodic simulation cell with the average size of 47×43×112 $Å^3$. The interlayer distance between the graphene sheets in this work is consistent with the experimental data for hydrated graphene systems (~12 Å) [126]. The same distance was used for both 2NPG and 2NPGO systems for a valid comparison between them. A mixture of CO_2 and CH_4 (a total of 1,000 molecules) with different CH_4 concentrations (0, 25, 50, 75, and 100 mol% corresponding to 0, 250, 750, and 1000 CH_4 molecules) were then packed above the NPG or NPGO sheets using the Amorphous Cell module of Materials Studio.

Representative initial structures of single- and double-layered NPG membranes with 50 mol% CH_4 in the CH_4/CO_2 mixture are shown in Figures 3.1c and 3.1d, respectively. Since the pore sizes and interlayer spacing between the NPG or NPGO sheets in our models are larger than the kinetic diameters of CO_2 and CH_4 (3.30 and 3.80 Å, respectively) [127], gas molecules of both species are able to permeate through the membranes. Moreover, it is known that gas diffusion through the membrane separation is important when the pore diameter is in the range of 10-20 Å [128]; hence, the pore size was fixed in this work at a value that would be within this range (a = 10.0 Å, b = 12.3 Å). All in all, 20 different systems were created.

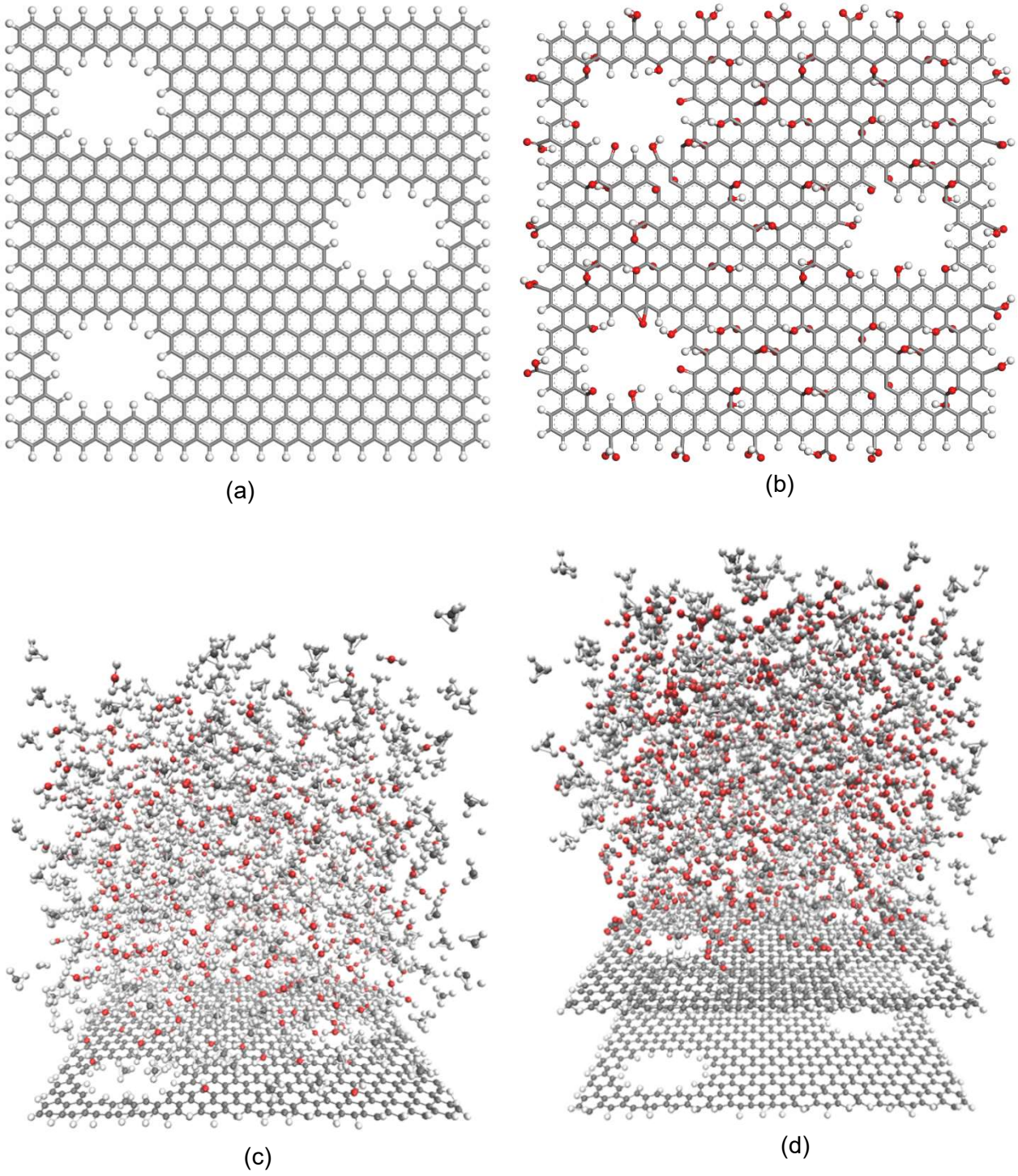

Figure 3. 1. Representative schematics of (a) a porous NPG and (b) a porous NPGO sheet, as well as the initial configurations of (c) a single-layered NPG and (d) a double-layered NPG membrane system with 50 mol% CH_4 in the CH_4/CO_2 mixture. The elliptic pores are all the same size (a = 6.2 Å, b = 4.9 Å). The interlayer spacing in the double-layered NPG and NPGO membrane systems is 12.4 Å.

The above structures were then exported to the LAMMPS [129] software package (version: March 2016). Subsequently, they were energy-minimized using the Conjugate Gradient method [130]. Next, an NVE (constant number of atoms, N; constant volume, V; constant energy, E) simulation was run for the different systems using the COMPASS force field[131] with a time step of 1 fs and a cut-off distance of 12 Å for a total simulation time of 120 ns. The temperature for all systems were controlled by a Langevin thermostat [132]. COMPASS force field has been parameterized for alkanes [131] and CO_2 [133], and has been used in the past for the dynamics simulations of systems composed of graphene and graphene oxide [124,125]. It is, therefore, deemed suitable for the simulation of CH_4/CO_2 gas separation in NPG and NPGO membranes.

As a measure of CO_2 and CH_4 affinity with the membranes, a potential of mean force (PMF) analysis [134] was performed for a single CO_2 (or CH_4) molecule approaching and penetrating the center of a single pore on a single NPG (or NPGO) layer. A spring with a constant of 100 kcal/mol-Å^2 was tethered to the center of mass of the pore on the graphene sheet, which was fixed in the *xz* plane, and the molecule was made to move in the *y*-direction from an initial separation distance of 6 Å to -6 Å (through the pore and to the other side of the graphene sheet) with a distance increment of 0.3 Å. At each distance increment, the pore's center of mass and the CO_2 (or CH_4) molecule were fixed in the *y*-direction and an NPT (constant number of atoms, N; constant pressure, P; constant temperature, T) simulation was run for 500 ps to equilibrate the system. Since the pore's center of mass and the CO_2 (or CH_4) molecule are at force equilibrium at each increment, the PMF can be calculated using the following formula:

$$PMF(d) = \int_{d_1}^{d_2} \langle F(r) \rangle dr \tag{3.1}$$

where d is the distance between the pore's center of mass and the CO_2 (or CH_4) molecule, r is the reaction coordinate, and $\langle F(r) \rangle$ is the average spring force applied to the pore's center of mass and the CO_2 (or CH_4) molecule.

3.4. Results and Discussion

In this section, the adsorption and transport properties of CH_4 and CO_2 in single- and double-layered NPG and NPGO membranes are presented.

3.4.1. Gas Adsorption Capacity.

In Figure 3.2, the CO_2 and CH_4 mass densities as a function of distance from the membrane surface (gas adsorption capacities) are given for the single-layered NPG and NPGO membranes and different CH_4 concentrations in the CH_4/CO_2 mixture. For the gas side of the membranes, the near-surface CO_2 concentration is found to be much larger than that of CH_4 for all CH_4 concentrations, indicating that a higher adsorption capacity of CO_2 on the membrane is realized versus that of CH_4. For both membranes and all CH_4 concentrations, except 75 mol%, there are at least two layers of CO_2 (two or more peaks in Figure 3.2) on the gas side of the membrane up to a distance of about 3 nm from the membrane surface. This distance is referred to as the Gibbs dividing surface [135–139], on which the gas species' concentration differs in the layers by at least 5%. These CO_2 layers are formed because of the frequent adsorption and desorption of the CO_2 molecules on the membrane surface. For the higher CH_4 concentration of 75 mol% (Figure 3.2d), only one layer of CO_2 is formed, since a smaller number of CO_2 molecules is available for adsorption on the membrane surface. Moreover, on the vacuum side of both membranes, only one

layer of CO_2 is formed (Figure 3.2). For all concentrations of CH_4, no CH_4 layers are observed on either side of the membranes, since all gas molecules are uniformly distributed on the membrane surface. For the pure CH_4 system (Figure 3.2e), one thin CH_4 layer (one peak) is observed to form on both the gas and vacuum sides of the NPG membrane only. Similar adsorption capacity trends are reported by Trinh et al. [138] for the adsorption of CO_2 and CH_4 on a mesoporous carbon surface.

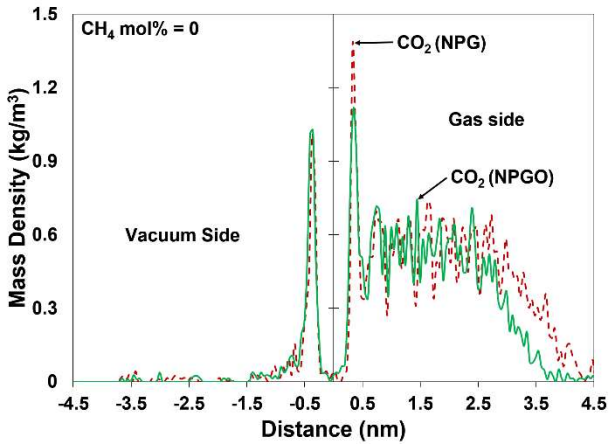
CH4 mol% = 0
CO2 (NPG)
Gas side
CO2 (NPGO)
Vacuum Side
Mass Density (kg/m3)
Distance (nm)

(a)

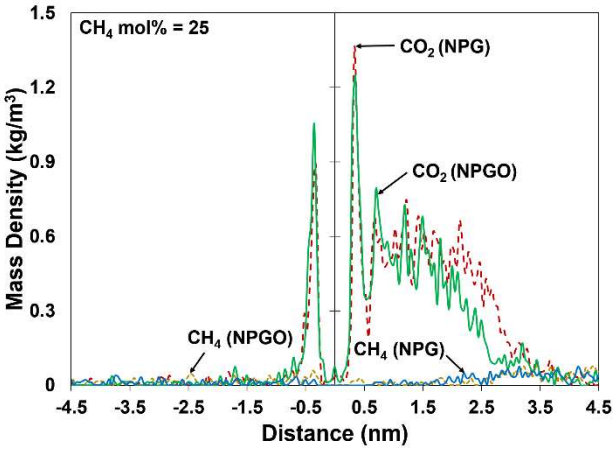
CH4 mol% = 25
CO2 (NPG)
CO2 (NPGO)
CH4 (NPGO)
CH4 (NPG)
Mass Density (kg/m3)
Distance (nm)

(b)

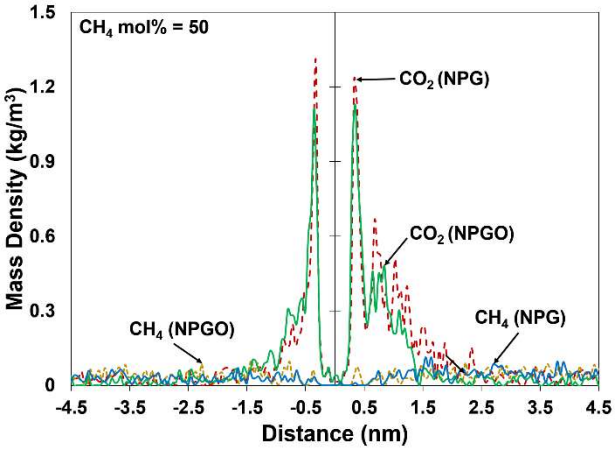
CH4 mol% = 50
CO2 (NPG)
CO2 (NPGO)
CH4 (NPGO)
CH4 (NPG)
Mass Density (kg/m3)
Distance (nm)

(c)

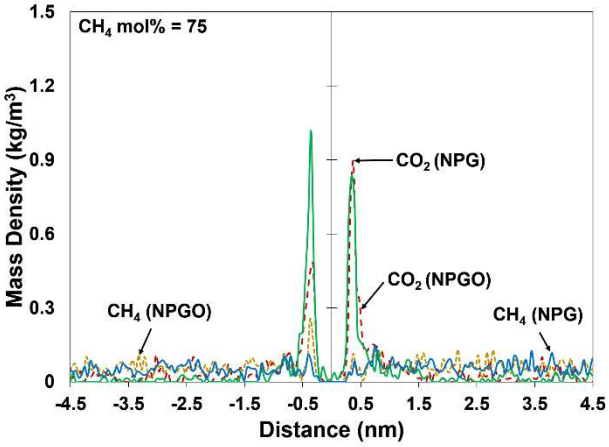
CH4 mol% = 75
CO2 (NPG)
CO2 (NPGO)
CH4 (NPGO)
CH4 (NPG)
Mass Density (kg/m3)
Distance (nm)

(d)

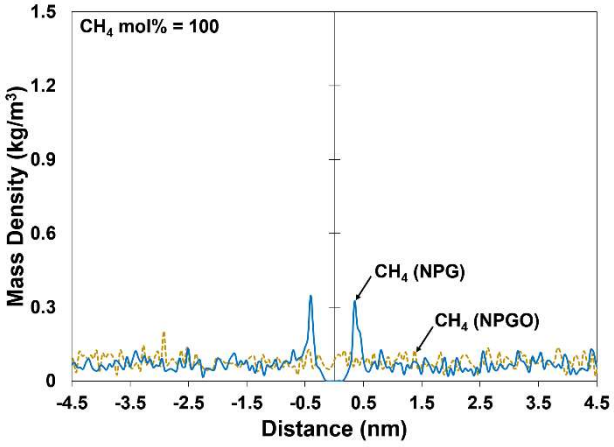
CH4 mol% = 100
CH4 (NPG)
CH4 (NPGO)
Mass Density (kg/m3)
Distance (nm)

(e)

Figure 3. 2. Mass densities of CO_2 and CH_4 on the gas side (positive distance values) and vacuum side (negative distance values) of the single-layered NPG and NPGO membranes at the CH_4 concentrations of (a) 0 mol%, (b) 25 mol%, (c) 50 mol%, (d) 75 mol%, and (e) 100 mol% in the CH_4/CO_2 mixture.

The above observations are better explained by comparing the affinities of CO_2 and CH_4 to the NPG and NPGO surface pores, determined by a PMF analysis (see the Computational Methods section). The PMF results are given in Figure 3.3. By investigating this figure, the CH_4 molecule is found to have a negligible affinity to both the NPG and NPGO sheets, as evident from its average PMF values being close to zero at all CH_4-pore distances, contrary to the CO_2 molecule. The high affinity of the latter molecule to the membrane pore is due to the presence of large interactions between the polar CO_2 molecule and the highly charged pore cavity, where hydrogenated and/or oxygenated functional groups exist on the pore rim. The low affinity of the CH_4 molecule to the NPG and NPGO layers makes it easier for this molecule to permeate through the membrane, resulting in a poor selectivity for the CO_2/CH_4 separation, but a good selectivity for the CH_4/CO_2 separation. This point will be revisited later.

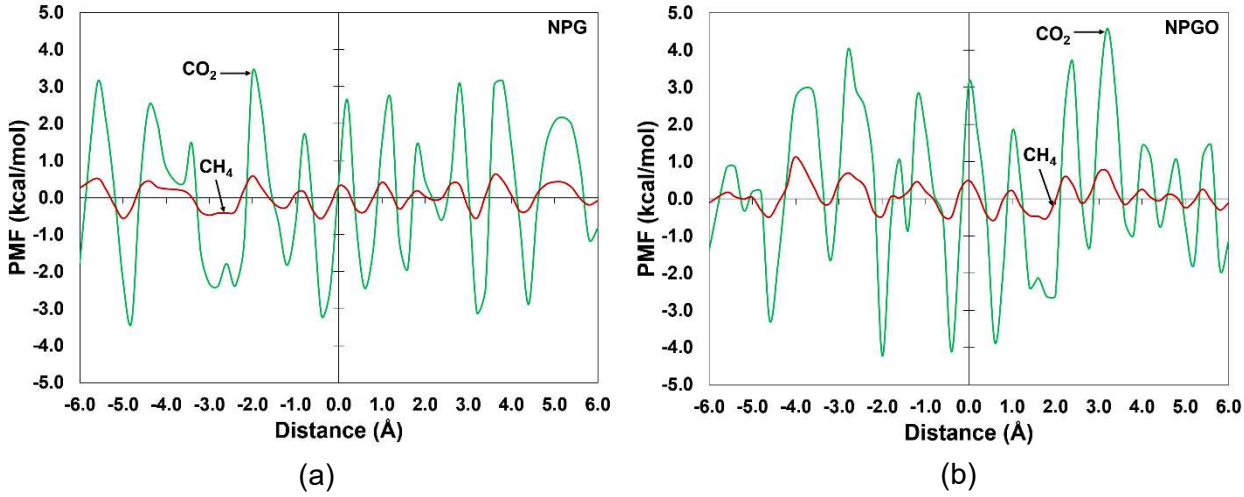

Figure 3. 3. Potential of mean force (PMF) between a single CO_2 (and CH_4) molecule and a pore on (a) a single NPG and (b) a single NPGO sheet.

In Figure 3.3, the adsorption capacity of CO_2 and CH_4 on the double-layered NPG and NPGO membranes are compared at different CH_4 concentrations. At low CH_4 concentrations (< 50 mol%), at least three layers of CO_2 are formed on the gas side of the membranes (three or more peaks in Figures 3.4a and 3.4b). This observation is attributed to the high affinity of the CO_2 molecules to the membranes, as a consequence of which these molecules are trapped in the membrane cavities and, hence, are prevented from passing through. In addition, one layer of CO_2 is formed on the vacuum side of the double-layered NPG and NPGO membranes, except for the pure CO_2. Contrary to the single-layered membranes, the CH_4 molecules form surface-adsorbed layers for the mixtures with 25 and 75 CH_4 mol% on the gas side of the double-layered membranes (Figures 3.4b-3.4d). This observation is attributed to the difficulty of the CH_4 diffusion through the double-layered NPG and NPGO membranes. Furthermore, for similar concentrations of CH_4

(25 and 75 mol%), there is one adsorbed layer of CH_4 on the vacuum side of all membranes (Figure 3.4).

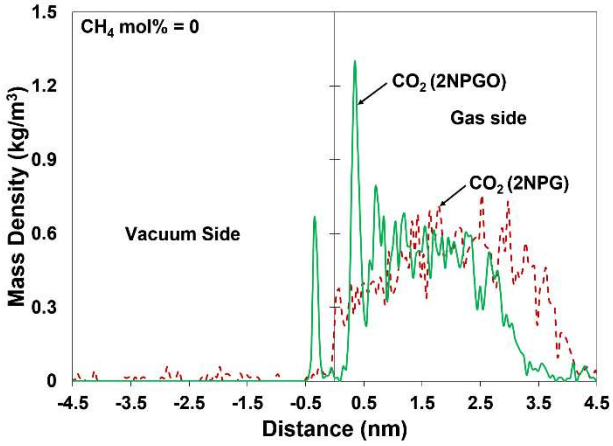
CH4 mol% = 0
CO2 (2NPGO)
Gas side
CO2 (2NPG)
Vacuum Side
Mass Density (kg/m3)
Distance (nm)

(a)

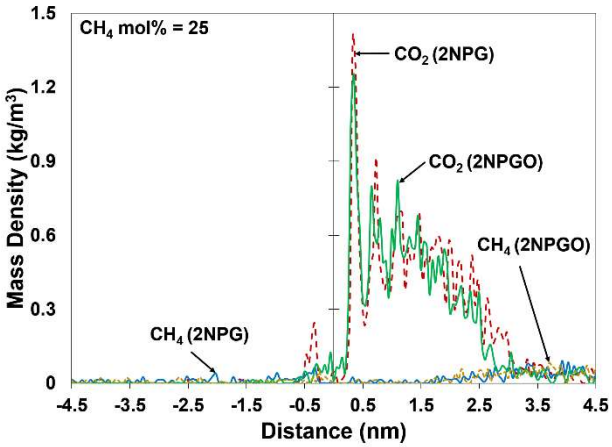
CH4 mol% = 25
CO2 (2NPG)
CO2 (2NPGO)
CH4 (2NPGO)
CH4 (2NPG)
Mass Density (kg/m3)
Distance (nm)

(b)

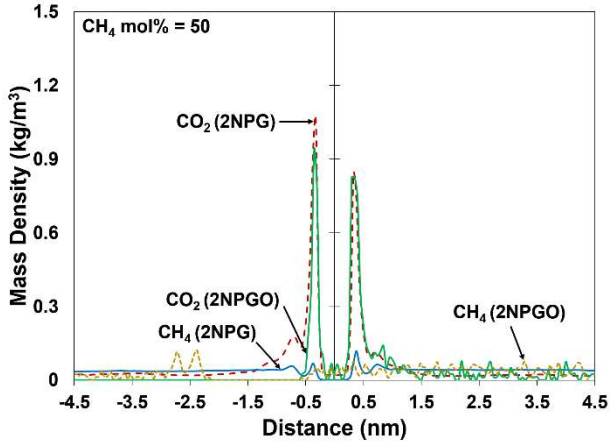
CH4 mol% = 50
CO2 (2NPG)
CO2 (2NPGO)
CH4 (2NPG)
CH4 (2NPGO)
Mass Density (kg/m3)
Distance (nm)

(c)

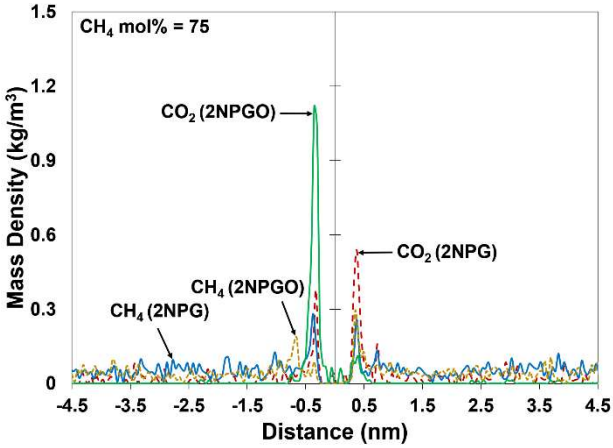
CH4 mol% = 75
CO2 (2NPGO)
CO2 (2NPG)
CH4 (2NPGO)
CH4 (2NPG)
Mass Density (kg/m3)
Distance (nm)

(d)

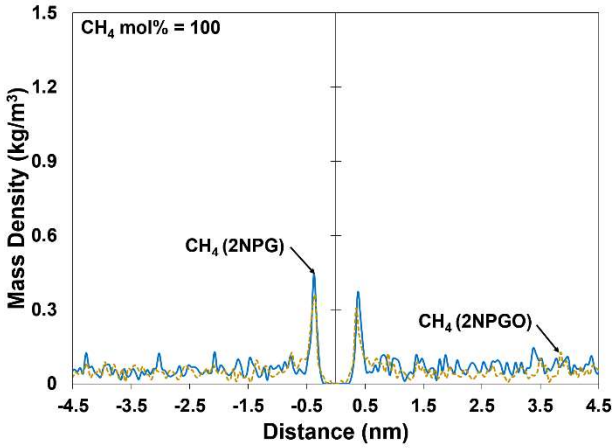
CH4 mol% = 100
CH4 (2NPG)
CH4 (2NPGO)
Mass Density (kg/m3)
Distance (nm)

(e)

Figure 3. 4. Mass densities of CO_2 and CH_4 on the gas side (positive distance values) and vacuum side (negative distance values) of the double-layered NPG and NPGO membranes at the CH_4 concentrations of (a) 0 mol%, (b) 25 mol%, (c) 50 mol%, (d) 75 mol%, and (e) 100 mol% in the CH_4/CO_2 mixture.

The adsorption isotherms for CO_2 and CH_4 on the single- and double-layered NPG and NPGO membrane surfaces at different CH_4 concentrations are shown in Figures 3.5 and 3.6, respectively. These isotherms are determined by calculating the number of adsorbed molecules on either side of the membrane divided by the membrane surface area as a function of gas side CO_2 or CH_4 partial pressure. The CO_2 adsorption reaches a limiting value at high CO_2 partial pressures (Figures 3.5a, 3.5b, 3.6a, and 3.6b); however, it generally drops with pressure for CH_4 (Figures 3.5c, 3.5d, 3.6c, and 3.6d). Consistent with the previous discussion on the adsorption capacity of the molecular species, CO_2 exhibits a higher adsorption on both single- and double-layered membrane surfaces than that of CH_4. For single-layered membranes (Figures 3.5a and 3.5b), the CO_2 adsorption is higher for the NPGO (Figure 3.5b) than that of NPG (Figure 3.5a) due to the presence of oxygenated functional groups on the membrane surface and pore rims of the former membrane. As previously discussed, the adsorption of CO_2 on both NPG and NPGO membranes decreases with an increase in the CH_4 concentration because of the presence of a smaller number of available CO_2 molecules for adsorption on the membrane surface. Moreover, the CO_2 adsorption sites on the membranes are occupied by an increasing number of CH_4 molecules. Trinh et al. [138] and You et al. [140] have reported similar observations for the CO_2 adsorption on the coal. The addition of another layer in the NPG and NPGO membranes has a large influence on the adsorption isotherms (Figures 3.5c, 3.5d, 3.6c, and 3.6d). For both single- and double-layered NPG and NPGO membranes (Figure 3.5), the CO_2 adsorption is nearly doubled for all CH_4 concentrations.

As for the CH_4 adsorption, none is observed on the NPG membrane (Figure 3.6a), while some adsorption occurs on the NPGO surface (Figure 3.6b). Contrary to the CO_2 adsorption (Figure 3.5), an increase in the CH_4 partial pressure causes the CH_4 adsorption to decrease (Figure 3.6). This behavior is attributed to the fact that CH_4 has, in general, less affinity to both NPG and NPGO membranes than that of CO_2 (Figures 3.2, 3.3, and 3.4). The addition of the second membrane layer nearly doubles the adsorption of CH_4 (Figure 3.6). You et al. [140] and Zhang et al. [122,141] have similarly obtained the adsorption isotherms for CH_4 on coal, which has graphite-like surface structures. They also report a drop in the CH_4 adsorption with an increase in the CH_4 partial pressure.

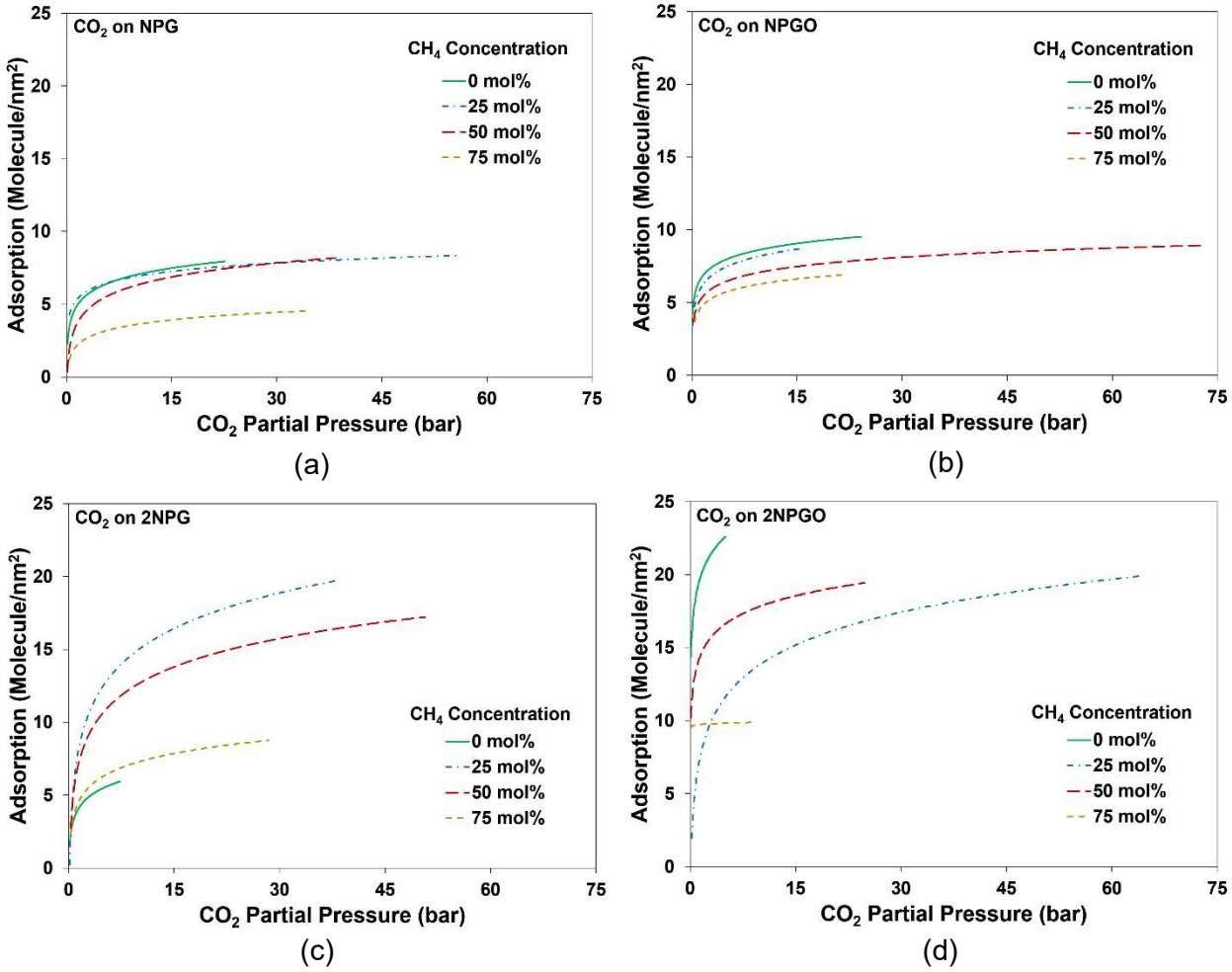

Figure 3. 5. Adsorption isotherms of CO_2 on (a) a single-layered NPG, (b) a single-layered NPGO, (c) a double-layered NPG (2NPG), and (d) a double-layered NPGO (2NPGO) membrane as a function of CO_2 partial pressure at different CH_4 concentrations.

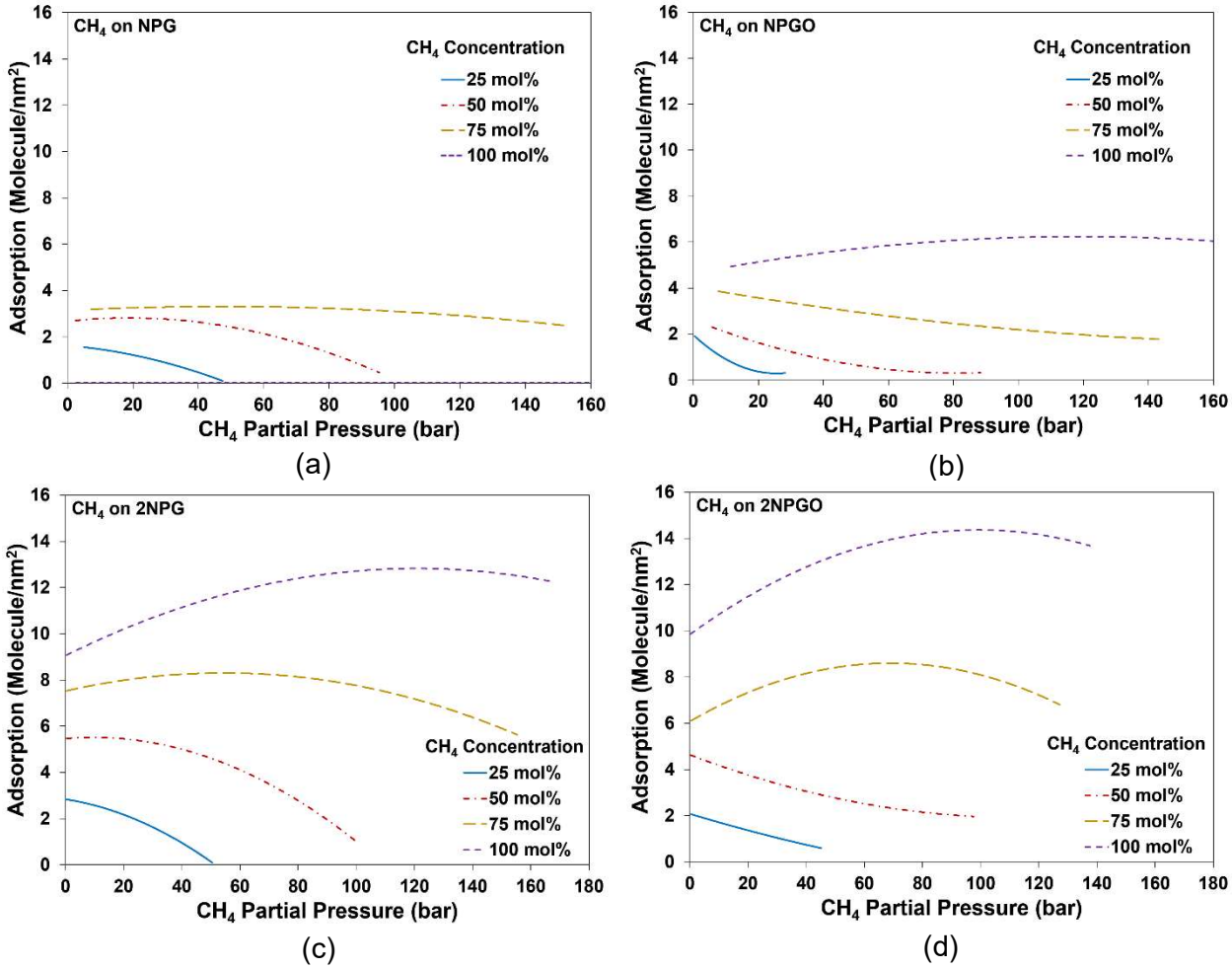

Figure 3. 6. Adsorption isotherms of CH_4 on (a) a single-layered NPG, (b) a single-layered NPGO, (c) a double-layered NPG (2NPG), and (d) a double-layered NPGO (2NPGO) membrane as a function of CH_4 partial pressure at different CH_4 concentrations.

3.4.2. Gas Transport Properties of the Membranes.

To examine the CH_4/CO_2 separation efficiency in the NPG and NPGO membranes, the diffusion coefficient, permeance, flow, and selectivity of the gaseous species were calculated.

3.4.2.1. Component Diffusion Coefficients.

In Figure 3.7, the mean-square displacement (MSD) data for the gas components in single- and double-layered NPG and NPGO membranes are given for 50 CH_4 mol%. In this figure, large limiting values of MSD indicate that the pore sizes are adequate to allow the molecular species to cross the membrane. A similar behavior is observed for all other systems (Figure 3.7).

A plot of MSD as a function of time should be linear if the diffusion coefficient of a penetrant molecule is constant [95,142–145] indicating an Einsteinian behavior. The diffusion coefficient (D) is calculated using a linear regression fit to the MSD data for the linear portion of the curve and applying the Einstein equation [146]:

$$D = \frac{1}{6}\lim_{t\to\infty}\frac{MSD}{t}, \tag{3.2}$$

where MSD is calculated based on the time-series of all atomic positions $\boldsymbol{r}$:

$$MSD \equiv \left\langle \left[\boldsymbol{r}(t) - \boldsymbol{r}(0)\right]^2 \right\rangle = \frac{1}{t}\sum_{t=t_0}^{t}\left[\boldsymbol{r}(t) - \boldsymbol{r}(0)\right]^2. \tag{3.3}$$

The CO_2 and CH_4 diffusion coefficients in single- and double-layered NPG and NPGO membranes are shown in Table 3.1. In general, CH_4 has a larger diffusion coefficient than that of CO_2 for all the different membrane configurations at low to intermediate CH_4 concentrations (< 50 mol%) (Table 3.1). This observation is attributed to the negligible affinity of the CH_4 molecule to the NPG and NPGO membranes versus that of the CO_2 molecule (Figures 3.2 and 3.3). Moreover, CH_4 has a smaller molecular weight than that of CO_2, resulting in a higher CH_4 molecular velocity. However, the CO_2 diffusion coefficients for the CH_4/CO_2 mixtures with 50 and 75 CH_4 mol% in the double-layered NPGO membrane are larger than those of CH_4 (Table 3.1). This may be attributed to the high CH_4 flux, favoring a convective transport of CO_2 thorough the double-layered

NPGO membrane. Our calculated CH_4 diffusion coefficients in graphene surfaces (Table 3.1) are in a good agreement with those published by Zhang et al. [122] Also, while the agreement between the CO_2 diffusion coefficients calculated in this work and those published by Sun and Bai [120] are good, our calculated CH_4 diffusion coefficients are smaller than those reported by them (4×10^{-7} m^2/s).

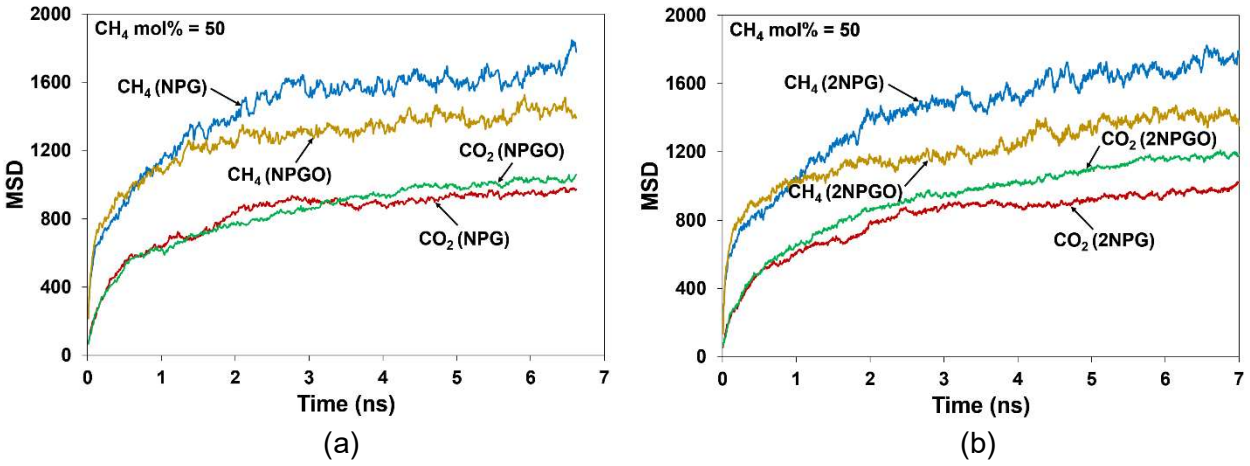

Figure 3. 7. Mean-square displacement (MSD) as a function of simulation time for CO_2 and CH_4 in (a) single-layered NPG and NPGO membranes and (b) double-layered NPG and NPGO membranes. The CH_4 concentration in the CH_4/CO_2 mixture is 50 mol%.

Table 3. 1. Calculated diffusion coefficients ($\times 10^{-9}$ m^2 s^{-1}) for CO_2 and CH_4 in NPG and NPGO membranes

Membrane	NPG		2NPG		NPGO		2NPGO	
Gas → / CH_4 (mol%)	CO_2	CH_4	CO_2	CH_4	CO_2	CH_4	CO_2	CH_4
0	1.02 ± 0.04	0.00	1.04 ± 0.02	0.00	1.19 ± 0.04	0.00	0.75 ± 0.02	0.00
25	0.87 ± 0.03	1.6 ± 0.1	0.71 ± 0.02	1.28 ± 0.06	0.88 ± 0.03	2.3 ± 0.1	0.73 ± 0.01	1.8 ± 0.1
50	1.05 ± 0.04	1.6 ± 0.1	1.01 ± 0.02	1.55 ± 0.08	1.28 ± 0.04	1.03 ± 0.06	1.12 ± 0.02	1.07 ± 0.06
75	2.25 ± 0.08	2.6 ± 0.1	1.73 ± 0.06	1.82 ± 0.09	1.58 ± 0.05	1.88 ± 0.08	1.74 ± 0.07	1.7 ± 0.1
100	0.00	3.3 ± 0.1	0.00	1.73 ± 0.08	0.00	2.1 ± 0.1	0.00	1.9 ± 0.01

3.4.2.2. Permeance and Gas Flow.

Gas flux through membranes for a given pore size depends on the kinetic diameter and molecular weight of the gaseous species, as well as the strength of their interactions with the membrane surface [101]. To visually inspect the permeation of CO_2 and CH_4 molecules through a single-layered NPGO membrane, the instantaneous system snapshots are given in Figure 3.8 for the equimolar mixture of CO_2 and CH_4 at three different simulation times. As observed in Figure 3.8a, the CO_2 molecules first adsorb on the membrane surface and pore rims and then, after saturating the surface and forming the adsorption layers (Figure 3.2c), penetrate the membrane from the gas side to the vacuum side. On the other hand, the permeation of CH_4 molecules (Figure 3.8b) through the NPGO membrane is rather unhindered without any appreciable surface adsorption of the CH_4 molecules.

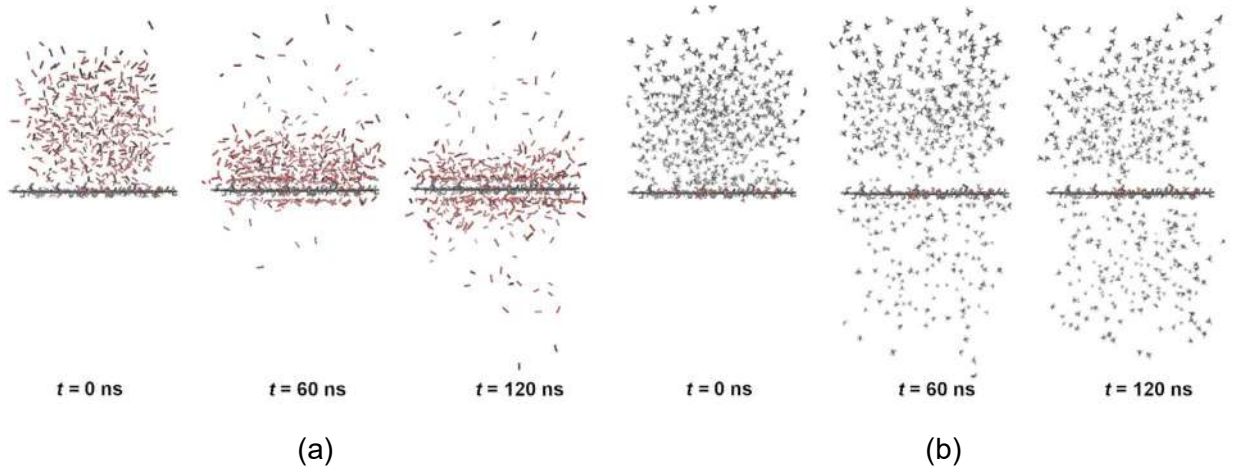

Figure 3. 8. Instantaneous system snapshots at initial (t = 0 ns), intermediate (t = 60 ns), and final (t = 120 ns) simulation times for (a) CO_2 and (b) CH_4 molecules permeating through a single-layered NPGO membrane. The CH_4 concentration is 50 mol%.

Ideally, both high permeance and high selectivity are required for the optimal separation performance of a membrane; however, in practice, there is a trade-off between these two properties. Permeance is defined by the flux of a specific gas passing through a membrane. In this work, the permeances for the different membranes (Table 3.2) are determined using the method described by Sun et al. [101] In this method, the gas flux is determined from the following formula [101]:

$$J' = \frac{1}{N_A}\frac{dN}{dt} = PA\Delta P, \tag{3.4}$$

where J' is the CO_2 or CH_4 flux, N_A is Avogadro's constant, N is the number of CO_2 or CH_4 molecules passing through the membrane, t is time, P is permeance, A is the total membrane area,

and ΔP is the partial pressure drop across the membrane. ΔP is determined by the pressure difference between the gas and vacuum sides of the membrane [101]:

$$\Delta P = \frac{N_i - N_{ad} - 2N}{N_i} p_i , \tag{3.5}$$

where N_i is the initial number of CO_2 or CH_4 molecules, N_{ad} is the number of adsorbed CO_2 or CH_4 molecules on both sides of the membrane, and p_i is the initial CO_2 or CH_4 pressure. N_{ad} is almost constant during the quasi-steady state period, because the total number of species molecules on both sides of the membrane remains constant. Also, the partial pressure drop in one side leads to an increase in the partial pressure on the other side [101]. After combining Equations 4 and 5 and solving for the resulting differential equation, the following formula is obtained for the number of gas molecules passing through the membrane:

$$N = \left(\frac{N_i - N_{ad}}{2} \right) \left(1 - e^{-\frac{PAN_A p_i t}{N_i}} \right). \tag{3.6}$$

The permeance can be determined using Equation 6 in combination with a nonlinear regression of the N versus t data. As observed in Table 3.2, the permeance of CO_2 is smaller than that of CH_4 for all membranes. Among both single- and double-layered NPG and NPGO membranes, the former exhibits the highest permeance for CO_2 at 75 CH_4 mol% due to a lower CO_2 adsorption capacity on this membrane (Figure 3.2d). Moreover, the double-layered NPGO membrane has the lowest permeance for CO_2 at the same CH_4 concentration. Since nearly all CO_2 molecules are adsorbed on the gas and vacuum sides of the double-layered NPGO membrane (Figure 3.4d), there are no more CO_2 molecules left to permeate the membrane. This leads to a lower permeance value (Table 3.2). When comparing the trend for CO_2 permeance as a function of CH_4 concentration among all membranes, an increase in the CH_4 concentration leads to an increase in the CO_2

permeance (Table 3.2). Similarly, an increase in the CH_4 concentration causes an increase in the CH_4 permeance for all membranes. The above observations are attributed to the fact that the probability for the CO_2 molecules to be carried through the membrane at higher CH_4 concentrations is higher. In other words, since the CH_4-membrane interactions are much weaker than those of CO_2-membrane (Figure 3.3), the higher number of CH_4 molecules at high CH_4 concentrations generally disrupts the favorable CO_2-membrane interactions and, ultimately, the convective CO_2 mass transport dominates. The presence of a second NPG or NPGO layer in the double-layered membranes leads to a large decrease in both CO_2 and CH_4 permeances (Table 3.2). The CO_2 permeances through the NPG membrane calculated herein are smaller than those published by Liu et al. [123]. The discrepancy between these results may be due to the use of different pore sizes, pore rim functional groups, and permeance calculation method in this work than those used by Liu and his coworkers. However, the permeance data obtained in this work agree well with those published by Sun et al. [101].

Table 3. 2. Gas permeances ($\times 10^3$ GPUs[a]) in NPG and NPGO membranes

Membrane	NPG		2NPG		NPGO		2NPGO	
Gas → / CH_4 mole%	CO_2	CH_4	CO_2	CH_4	CO_2	CH_4	CO_2	CH_4
0	27 ± 6	0	45 ± 1	0	29 ± 1	0	0.56 ± 0.01	0
25	29 ± 2	640 ± 20	33 ± 1	227 ± 4	54 ± 1	650 ± 10	38 ± 1	258 ± 3
50	120 ± 2	764 ± 20	43 ± 3	470 ± 10	186± 2	142 ± 5	48 ± 3	179 ± 1
75	527 ± 5	1120 ± 30	41 ± 3	713 ± 4	219 ± 5	429 ± 10	50 ± 1	171 ± 7
100	0	7140 ± 50	0	522 ± 6	0	640 ± 30	0	510 ± 10

[a] 1 GPU ≈ 3.35×10^{-10} mol m^{-2} Pa^{-1} s^{-1}

The molecular flow was also calculated in this work based on the following formula [95,96]:

$$F = \frac{N}{At} \tag{3.7}$$

where F is the molecular flow (mol m^{-2} s^{-1}), N is the number of moles of the permeating gas through the membrane, A is the total membrane area (m^{-2}), and t is the simulation time (s).

The flow of CO_2 and CH_4 through the membranes at different CH_4 concentrations (after 120 ns of simulation) are given in Figure 3.9. As expected, the flow of CO_2 shows a downward trend with an increase in the CH_4 concentration (Figure 3.9a). On the contrary, the flow of CH_4 increases with an increase in the CH_4 concentration (Figure 3.9b), signifying a similar trend of increase in CH_4 permeance with an increase in the CH_4 concentration.

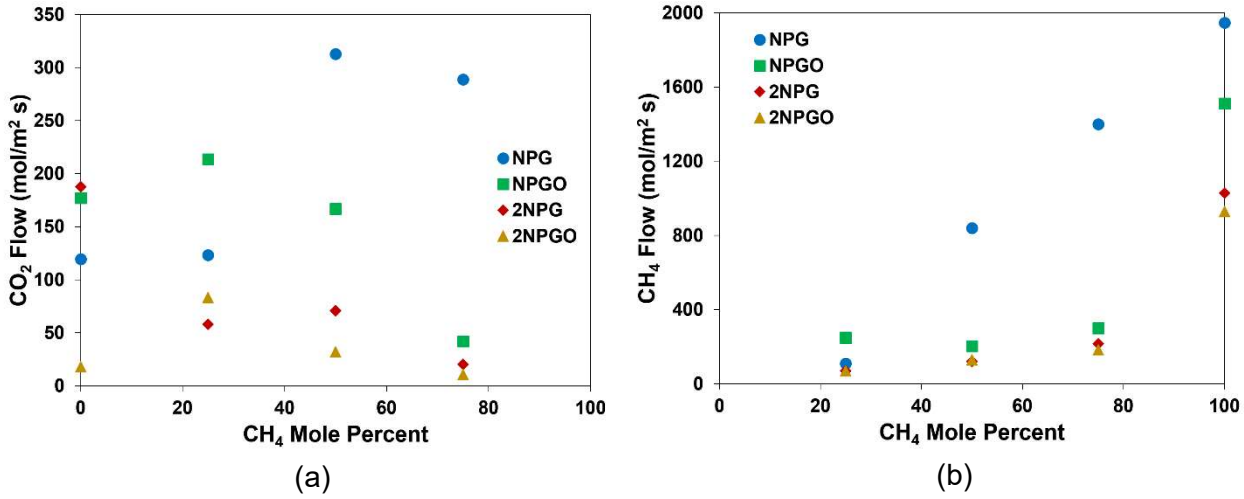

Figure 3. 9. Flow of (a) CO_2 and (b) CH_4 gases through the single- and double-layered NPG and NPGO membranes as a function of the CH_4 concentration

.

3.4.2.3. Membrane Selectivity

Since the permeation of CH_4 through the NPG and NPGO membranes is higher than that of CO_2 (Table 3.2), the CH_4/CO_2 separation selectivities are reported herein instead of those of the

CO_2/CH_4 separation. Traditionally membrane selecitivies are defined as the ratio of the individual permeances of the gases in the separations pair. For systems were both the feed and permeate chambers are well mixed (figure 3.8) the traditional definition can be reduce to the ratio of molecular content [6,99]:

$$S_{CH_4/CO_2} = \frac{\left(\frac{N_{CH_4}}{N_{CO_2}}\right)_{Vacuum}}{\left(\frac{N_{CH_4}}{N_{CO_2}}\right)_{Gas}}, \tag{3.8}$$

where S is the membrane selectivity.

In Figure 3.10, the instantaneous membrane selectivity of the CH_4/CO_2 separation is given as a function of simulation time for the single- and double-layered NPG and NPGO membranes at 50 CH_4 mol%. As seen in this figure, the membrane selectivity reaches a quasi-steady-state value after about 30 ns and 50 ns for the single- (Figure 3.10a) and double-layered (Figure 3.10b) NPG and NPGO membranes, respectively. The total number of gas molecules passing through the NPG and NPGO membranes (after 120 ns of simulation) and the steady-state membrane selectivities are given in Tables 3.3 and 3.4, respectively. The first row in Table 3.4 is determined based on the permeance of pure CO_2 and CH_4.

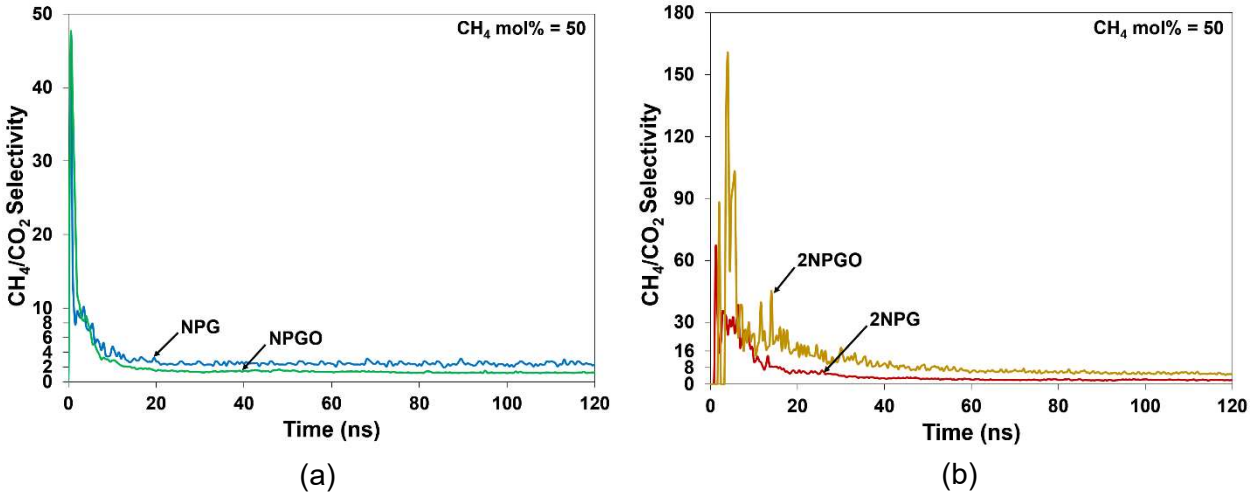

Figure 3. 10. Instantaneous membrane selectivity of the CH_4/CO_2 separation as a function of simulation time for (a) single-layered NPG and NPGO membranes and (b) double-layered NPG and NPGO membranes. The CH_4 concentration is 50 mol%.

Table 3. 3. Total number of gas molecules passing through the NPG and NPGO membranes after 120 ns of simulation

Membrane	NPG		2NPG		NPGO		2NPGO	
Gas → / CH_4 mole%	CO_2	CH_4	CO_2	CH_4	CO_2	CH_4	CO_2	CH_4
0	33	0	49	0	56	0	9	0
25	74	118	87	103	62	72	136	112
50	82	221	128	217	191	234	60	241
75	72	349	31	325	50	357	16	281
100	0	485	0	368	0	429	0	336

Table 3. 4. Quasi-steady-state membrane selectivity (S) of the NPG and NPGO membranes for the CH_4/CO_2 separation.

CH_4 mole%	Membrane			
	NPG	2NPG	NPGO	2NPGO
25	5.00	3.84	3.70	2.63
50	2.70	1.69	1.22	4.00
75	1.61	3.70	2.38	5.88

All membrane selectivities are larger than one (Table 3.4), indicating that the separation efficiency of NPG and NPGO membranes are satisfactory for the CH_4/CO_2 separation. It should be noted here that, to the best of our knowledge, no data are available in the literature for the CH_4/CO_2 separation in NPG or NPGO membranes. However, Shan et al. [147] and Wu et al. [99] have determined the selectivities for the CO_2/N_2 separation in NPG membranes and their selectivities are less than one for all their membrane configurations, suggesting that, similar to the work presented here for the CH_4/CO_2 separation, the NPG membranes are suitable for the N_2/CO_2 and not CO_2/N_2 separation.

As shown in Table 3.4, the NPGO membranes, in both single- and double-layered configurations, exhibit a better separation efficiency for the CH_4/CO_2 mixture than those of the single- and double-layered NPG membranes. The better performance of the NPGO membrane is attributed to the polarity and high affinity of the CO_2 molecules to the oxygen-containing functional groups on the membrane surface and pore rims (Figure 3.2).

The highest membrane selectivity is observed for the double-layered NPGO membrane at the 75 CH_4 mol%, while the lowest is observed for the single-layered NPGO membrane at 50 CH_4 mol% (Table 3.4). Again, similar to the permeance results in the previous section, the nearly complete adsorption of the CO_2 molecules on the gas side of the double-layered NPGO membrane (Figure

3.4d) leads to a higher membrane selectivity. Addition of a second layer to the NPGO membrane generally improves the membrane selectivity for the CH_4/CO_2 separation (at least for CH_4 concentrations > 25 mol%) (Table 3.4). On the contrary, the separation performance is generally deteriorated for the NPG membranes, except at high CH_4 concentrations (> 50 mol%). This observation is also related to the level of CO_2 adsorption on the NPGO membrane surface and pores, which increases with an increase in the number of membrane layers (Figures 3.2 and 3.4). An increase in the CH_4 concentration up to intermediate levels generally causes a decrease in the membrane selectivity (Table 3.4).

3.5. Conclusions

The performance of single- and double layered nanoporous pristine graphene (NPG) and graphene oxide (NPGO) as either adsorbents or membranes was explored for the CH_4/CO_2 separation using molecular dynamics simulation. Moreover, the adsorption capacity and adsorption isotherms of CO_2 and CH_4, as well as the CH_4 and CO_2 transport properties through the single- and double layered NPG and NPGO membranes were determined. These properties include the gas component diffusion coefficients, permeances, flows, and membrane selectivities, and adsorption isotherms for the CH_4/CO_2 separation.

An investigation of the adsorption capacities of CO_2 and CH_4 on the single- and double-layered NPG and NPGO membranes reveals that at least two layers of CO_2 are formed on the gas side of these materials. For all the NPG materials, CO_2 has the highest adsorption capacity, which further increases in NPGO materials because of the presence of oxygenated functional groups on the surface, edges, and pore rims. In addition, the adsorption of CO_2 decreases when the CH_4

concentration increases. While there is no adsorption for pure CH_4 on the single-layered NPG membrane, increasing the CH_4 concentration in the CH_4/CO_2 mixture enhances the CH_4 adsorption. The addition of a second layer to both NPG and NPGO materials increases the adsorption capacity of both CO_2 and CH_4.

The diffusion coefficients of both CO_2 and CH_4 increase when the CH_4 concentration increases for the single- and double-layered NPG and NPGO membranes. Furthermore, the addition of another NPG or NPGO layer causes a decrease in the diffusion coefficients for nearly all CH_4 concentrations. The permeance of CO_2 is smaller than that of CH_4 for all membranes. This suggests that the NPG and NPGO membranes perform well for the CH_4/CO_2 separation, but not for the CO_2/CH_4 separation. For all membranes, the membrane selectivities are higher than one, indicating that the CH_4/CO_2 separation efficiency in NPG and NPGO membranes are satisfactory. Moreover, the single- and double-layered NPGO membranes exhibit better membrane selectivity for the CH_4/CO_2 separation than that of the single- and double-layered NPG membranes. For the separation of CO_2 from CH_4 (with the desire to maintain CH_4 at high pressure), the simulated separation platforms in this work prove to be better CO_2 adsorbents than CO_2/CH_4 separation membranes. The molecular insights obtained in this work on the CH_4/CO_2 gas separation in nanoporous graphene-based membranes can be extended to other gas separations in these membranes using the developed methodology.

CHAPTER IV

CONCLUSIONS

Membranes for gas separation are studied both experimentally and computationally in this dissertation. The main objective of this study was gas separation using membranes for natural gas upgrading in which special attention is given for the separation of high value hydrocarbons such as propane (C_3H_8) from natural gas and carbon dioxide (CO_2) separation from light gases such as nitrogen (N_2) and methane (CH_4). Different types of membranes such as supported ionic liquid membranes (SILMs), biphasic membranes, and nanoporous graphene (NPG) and graphene oxide (NPGO) membranes are studied.

The biphasic membranes are proposed to overcome SILMs issues for gas separation. The biphasic membranes were characterized using FTIR tests and AFM imaging. The FTIR tests showed strong interactions of [emim][SCN] with CA molecules with the hydrogen bonding, Coulombic forces, and van der Waals interactions. The CA dissolving in [emim][SCN] is strongly affected by these interactions. The gas transport properties of CO_2, N_2, CH_4, and C_3H_8 through the biphasic membrane were measured. In order to assess the gas separation performance of the biphasic membrane, the permeabilities of the above mentioned gases through the dope and SILM membranes are also obtained. The results show that the permeability of CO_2, CH_4, and N_2 is close to those for SILM using the same RTIL. The SILM showed the highest permeability for CO_2 and C_3H_8, while the dope membrane was slowest permeable membrane for CO_2 and C_3H_8. In addition,

the study of selectivity for biphasic membranes shows that the separation performance of biphasic membrane is close to SILM. The stability of the biphasic and SILM membranes are examined as a function of retentate pressure and the results showed that the biphasic and SILM membranes have similar breakthrough points.

The main objective of this study is natural gas processing and novel materials such as graphene is selected. NPG and NPGO sheets were studied computationally due to the lack of synthesizing data for NPG and NPGO. For the efficient separation of CO_2 from methane, single- and double-layered NPG and NPGO membranes are studied. The adsorption and transport properties of the CO_2 and CH_4 through the NPG and NPGO membranes are determined. The results show that an at least two layers of CO_2 are formed on the gas side of these materials. For all of the films, CO_2 has the highest adsorption capacity and further increases with the presence of oxygenated functional groups in NPGO membranes. CH_4 concentration has a negative effect on the CO_2 adsorption. The adsorption capacity of addition of both CO_2 and CH_4 increases by addition of a second layer of both NPG and NPGO films. An increase in the CH_4 concentration leads to an increase to the diffusion coefficients of both CO_2 and CH_4 for all of the configurations. Furthermore, the addition of another NPG or NPGO layer causes a decrease in the diffusion coefficients for nearly all CH_4 concentrations. The permeance of CO_2 is smaller than that of CH_4 for all films. This suggests that the NPG and NPGO membranes perform well for the CH_4/CO_2 separation, but not for the CO_2/CH_4 separation. Moreover, the single- and double-layered NPGO membranes exhibit better membrane selectivity for the CH_4/CO_2 separation than that of the single- and double-layered NPG membranes. For the separation of CO_2 from CH_4 (with the desire to maintain CH_4 at high pressure), the simulated separation platforms in this work prove to be better CO_2 adsorbents than CO_2/CH_4 separation membranes. The molecular insights obtained in this

work on the CH_4/CO_2 gas separation in nanoporous graphene-based membranes can be extended to other gas separations using the developed methodology.

Among the studied membranes, the biphasic membrane is promising for CO_2/CH_4 separation in terms of separation performance and cross-membrane pressure. In addition, the SILM membrane show promise for the reverse-selective separations such as C_3H_8/N_2 and C_3H_8/CH_4 separations. Moreover, the NPG and NPGO sheets show better performance as gas adsorbents that membranes.

CHAPTER V

FUTURE WORK

The studied biphasic membranes showed a good performance for gas separation application especially for the CO_2/N_2 and CO_2/CH_4 separations. However, these membranes have potential for improvement. The separation performance of biphasic membranes is highly dependent on the casting procedure and it needs modifications. The casting procedure must be modified in which the phase inversion of the cast film is slowly achieved since [emim][SCN] is miscible in the water. This will improve the gas transport properties of the biphasic membranes. The used procedure in this dissertation leaded to a fast phase inversion. The fast phase inversion leads to loose of [emim][SCN] into the water. To achieve slow and gradual phase inversion, three approaches can be used. The first approach is to use water as casting agent similar to this dissertation and determine an optimum time for the phase inversion. In this dissertation, several time periods were considered for the phase inversion, however due to the lack of time, optimum phase inversion time was not determined. Therefore, a comprehensive study of phase inversion time in water is necessary. The second approach is to use a different casting agent in which [emim][SCN] is partially miscible in the casting agent. The last approach is to use a mixture of casting agents to determine an optimum agent for casting and phase inversion of the biphasic membranes.

The membrane thickness has a large impact on the gas transport properties and mechanical stability of the membrane. The thicker membrane might have a better separation performance,

however at high pressures, the membrane will compact and leads to a decrease in the gas transport. Also, a thinner membrane might resolve the membrane compacting. But, there is a possibility for the membrane at high pressures to crash or RTIL displacement from the pores of the membrane. In addition, the effect of pressure on the polymer compacting in the RTIL-membranes has not been determined yet. Therefore, a comprehensive study of the membrane thickness at different pressures is needed.

The gas solubility in RTILs is strongly depends on the temperature. In addition, increase in the temperature intensifies CA solubility in [emim][SCN]. Furthermore, CA decomposition point is 90ºC. Therefore, the stability of the biphasic membranes strongly depends on the temperature. First, ternary diagrams must be determined at different temperatures to determine the stability of the CA/[emim][SCN] solution. The ternary diagrams can also be used to determine optimum casting temperature. Then, the stability of biphasic membrane must be examined at different temperatures to emphasize the membrane ability to withstand and operate at different temperatures.

To study the reverse-selectivity of the biphasic membranes, the continuous flow instrument should be modified in order to be able to test propane and butane transport properties at high pressures.

The NPG and NPGO films can be modified by using different functional groups such as fluorine groups. Functional groups have large impact on the gas adsorption and transport properties of the NPG films. The NPG films which was modified with fluorine groups showed better performance for the CO_2/N_2 and I think the testing NPG modified with fluorine groups is worth investigating. Furthermore, for single- and multi-layered NPG and NPGO, the effect of different

pore size on the gas transport through the sheets is necessary. Moreover, a single-layered NPG membrane with different pore sizes or a multi-layered NPG membrane with different pore sizes in an asymmetric configuration is an interesting subject to study. In addition, the location and arrangement of the NPG sheets in the multi-layered separation platforms will affect the gas adsorption and transport properties. Consequently, the study of multi-layered NPG separation platforms is another route to study.

In addition, the effect of number NPG or NPGO sheets on the gas transport and adsorption has not been studied yet. A comprehensive study of multilayered NPG and NPGO sheets is needed. For the multilayered NPG and NPGO sheets several gas adsorption and transport aspects can be investigated. First, the path of gas molecules through the NPG and NPGO sheets is an important parameter which requires further study. For example, gases like CO_2 will adsorb on the surface of NPG or NPGO, in contrast, CH_4 does not have any interaction with surface and can easily pass through the sheets. Therefore, the path of CO_2 molecules will be different than that of CH_4. Furthermore, the path of gas molecules through the NPG and NPGO sheets is strongly affected by the presence of functional groups on the surface. Therefore, similar study with different functional groups will emphasize the effect of functional groups on the gas transport path, adsorption, and transport.

LIST OF REFERENCES

[1] J. Black, Cost and Performance Baseline for Fossil Energy Plants, 2013.

[2] A. Khosravi, M. Sadeghi, Separation performance of poly(urethane–urea) membranes in the separation of C2 and C3 hydrocarbons from methane, J. Memb. Sci. 434 (2013) 171–183. doi:10.1016/j.memsci.2013.01.025.

[3] A. Khakpay, P. Scovazzo, Reverse-Selective Behavior of the Room Temperature Ionic Liquid Based Membranes for Natural Gas Processing, J. Memb. Sci. 545 (2018) 204–212. doi:https://doi.org/10.1016/j.memsci.2017.09.068.

[4] L. a. Neves, J.G. Crespo, I.M. Coelhoso, Gas permeation studies in supported ionic liquid membranes, J. Memb. Sci. 357 (2010) 160–170. doi:10.1016/j.memsci.2010.04.016.

[5] P. Uchytil, J. Schauer, R. Petrychkovych, K. Setnickova, S.Y. Suen, Ionic liquid membranes for carbon dioxide-methane separation, J. Memb. Sci. 383 (2011) 262–271. doi:10.1016/j.memsci.2011.08.061.

[6] P. Scovazzo, Determination of the upper limits, benchmarks, and critical properties for gas separations using stabilized room temperature ionic liquid membranes (SILMs) for the purpose of guiding future research, J. Memb. Sci. 343 (2009) 199–211. doi:10.1016/j.memsci.2009.07.028.

[7] P.K. Kilaru, R.A. Condemarin, P. Scovazzo, Correlations of Low-Pressure Carbon Dioxide and Hydrocarbon Solubilities in Imidazolium-, Phosphonium-, and Ammonium-Based Room-Temperature Ionic Liquids. Part 1. Using Surface Tension, Ind. Eng. Chem. Res. 47 (2008) 900–909. doi:10.1021/ie070836b.

[8] P.K. Kilaru, P. Scovazzo, Correlations of low-pressure carbon dioxide and hydrocarbon

solubilities in imidazolium-, phosphonium-, and ammonium-based room-temperature ionic liquids. Part 2. Using activation energy of viscosity, Ind. Eng. Chem. Res. 47 (2008) 910–919. doi:10.1021/ie070836b.

[9] J.J. Close, K. Farmer, S.S. Moganty, R.E. Baltus, CO2/N2 separations using nanoporous alumina-supported ionic liquid membranes: Effect of the support on separation performance, J. Memb. Sci. 390–391 (2012) 201–210. doi:10.1016/j.memsci.2011.11.037.

[10] J. Grünauer, S. Shishatskiy, C. Abetz, V. Abetz, V. Filiz, Ionic liquids supported by isoporous membranes for CO_2/N_2 gas separation applications, J. Memb. Sci. 494 (2015) 224–233. doi:10.1016/j.memsci.2015.07.054.

[11] F. Krull, C. Fritzmann, T. Melin, Liquid membranes for gas/vapor separations, J. Memb. Sci. 325 (2008) 509–519. doi:10.1016/j.memsci.2008.09.018.

[12] L.J. Lozano, C. Godínez, a. P. de los Ríos, F.J. Hernández-Fernández, S. Sánchez-Segado, F.J. Alguacil, Recent advances in supported ionic liquid membrane technology, J. Memb. Sci. 376 (2011) 1–14. doi:10.1016/j.memsci.2011.03.036.

[13] D. Camper, J. Bara, C. Koval, R. Noble, Bulk-Fluid Solubility and Membrane Feasibility of Rmim-Based Room-Temperature Ionic Liquids, Ind. Eng. Chem. Res. 45 (2006) 6279–6283. doi:10.1021/ie060177n.

[14] P. Scovazzo, J. Kieft, D. Finan, C. Koval, D. Dubois, R. Noble, Gas separations using non-hexafluorophosphate $[PF_6]-$ anion supported ionic liquid membranes, J. Memb. Sci. 238 (2004) 57–63. doi:10.1016/j.memsci.2004.02.033.

[15] D. Camper, C. Becker, C. Koval, R. Noble, Diffusion and Solubility Measurements in Room

Temperature Ionic Liquids, Ind. Eng. Chem. Res. 45 (2006) 445–450. doi:10.1021/ie0506668.

[16] A. Finotello, J. Bara, Room-temperature ionic liquids: temperature dependence of gas solubility selectivity, Ind. Eng. Chem. Res. 47 (2008) 3453–3459. doi:10.1021/ie0704142.

[17] J. Jacquemin, M.F. Costa Gomes, P. Husson, V. Majer, Solubility of carbon dioxide, ethane, methane, oxygen, nitrogen, hydrogen, argon, and carbon monoxide in 1-butyl-3-methylimidazolium tetrafluoroborate between temperatures 283K and 343K and at pressures close to atmospheric, J. Chem. Thermodyn. 38 (2006) 490–502. doi:10.1016/j.jct.2005.07.002.

[18] P. Scovazzo, D. Camper, J. Kieft, J. Poshusta, C. Koval, R. Noble, Regular Solution Theory and CO_2 Gas Solubility in Room-Temperature Ionic Liquids, Ind. Eng. Chem. Res. 43 (2004) 6855–6860. doi:10.1021/ie049601f.

[19] D. Camper, J. Bara, C. Koval, R. Noble, Bulk-Fluid Solubility and Membrane Feasibility of Rmim-Based Room-Temperature Ionic Liquids, (2006) 6279–6283.

[20] J.E. Bara, T.K. Carlisle, C.J. Gabriel, D.E. Camper, A. Finotello, D.L. Gin, R.D. Noble, Gas separations in fluoroalkyl-functionalized room-temperature ionic liquids using supported liquid membranes, 147 (2009) 43–50. doi:10.1016/j.cej.2008.11.021.

[21] P.J. Carvalho, J. a. P. Coutinho, The polarity effect upon the methane solubility in ionic liquids: a contribution for the design of ionic liquids for enhanced CO_2/CH_4 and H_2S/CH_4 selectivities, Energy Environ. Sci. 4 (2011) 4614. doi:10.1039/c1ee01599k.

[22] J.E. Bara, T.K. Carlisle, C.J. Gabriel, D. Camper, A. Finotello, D.L. Gin, R.D. Noble, Guide

to CO 2 Separations in Imidazolium-Based Room-Temperature Ionic Liquids, (2009) 2739–2751.

[23] D. Camper, C. Becker, C. Koval, R. Noble, Low Pressure Hydrocarbon Solubility in Room Temperature Ionic Liquids Containing Imidazolium Rings Interpreted Using Regular Solution Theory, Ind. Eng. Chem. Res. 44 (2005) 1928–1933. doi:10.1021/ie049312r.

[24] D.Y. Xing, N. Peng, T.S. Chung, Investigation of unique interactions between cellulose acetate and ionic liquid [EMIM][SCN], and their influences on hollow fiber ultrafiltration membranes, J. Memb. Sci. 380 (2011) 87–97. doi:10.1016/j.memsci.2011.06.032.

[25] I. Tirouni, M. Sadeghi, M. Pakizeh, Separation of C_3H_8 and C_2H_6 from CH_4 in polyurethane-zeolite 4Å and ZSM-5 mixed matrix membranes, Sep. Purif. Technol. 141 (2015) 394–402. doi:10.1016/j.seppur.2014.12.012.

[26] A. Khosravi, M. Sadeghi, Separation performance of poly(urethane-urea) membranes in the separation of C2 and C3 hydrocarbons from methane, J. Memb. Sci. 434 (2013) 171–183. doi:10.1016/j.memsci.2013.01.025.

[27] B. Lam, M. Wei, L. Zhu, S. Luo, R. Guo, A. Morisato, P. Alexandridis, H. Lin, Cellulose triacetate doped with ionic liquids for membrane gas separation, Polymer (Guildf). 89 (2016) 1–11. doi:http://dx.doi.org/10.1016/j.polymer.2016.02.033.

[28] A. Khakpay, F. Rahmani, S. Nouranian, P. Scovazzo, Molecular Insights on the CH_4/CO_2 Separation in Nanoporous Graphene and Graphene Oxide Separation Platforms: Adsorbents versus Membranes, J. Phys. Chem. C. 121 (2017) 12308–12320. doi:10.1021/acs.jpcc.7b03728.

[29] A.R. Moghadassi, Z. Rajabi, S.M. Hosseini, M. Mohammadi, Fabrication and modification of cellulose acetate based mixed matrix membrane: Gas separation and physical properties, J. Ind. Eng. Chem. 20 (2014) 1050–1060. doi:10.1016/j.jiec.2013.06.042.

[30] S. Hafeez, X. Fan, A. Hussain, A Kinetic Study of CO_2 Adsorption in Cellulose Acetate Membranes, Int. J. Environ. Sci. Dev. 6 (2015) 755–759. doi:10.7763/IJESD.2015.V6.694.

[31] R.W. Baker, K. Lokhandwala, Natural gas processing with membranes: An overview, Ind. Eng. Chem. Res. 47 (2008) 2109–2121. doi:10.1021/ie071083w.

[32] C.A. Scholes, G.W. Stevens, S.E. Kentish, Membrane gas separation applications in natural gas processing, Fuel. 96 (2012) 15–28. doi:10.1016/j.fuel.2011.12.074.

[33] N. Shahkaramipour, M. Adibi, A.A. Seifkordi, Y. Fazli, Separation of CO_2/CH_4 through alumina-supported geminal ionic liquid membranes, J. Memb. Sci. 455 (2014) 229–235. doi:https://doi.org/10.1016/j.memsci.2013.12.039.

[34] J.T. Vaughn, D.J. Harrigan, B.J. Sundell, J.A. Lawrence, J. Yang, Reverse selective glassy polymers for C3+ hydrocarbon recovery from natural gas, J. Memb. Sci. 522 (2017) 68–76. doi:10.1016/j.memsci.2016.09.003.

[35] M. Arruebo, J. Coronas, M. Menéndez, J. Santamaría, Separation of hydrocarbons from natural gas using silicalite membranes, Sep. Purif. Technol. 25 (2001) 275–286. doi:10.1016/S1383-5866(01)00054-5.

[36] A. Javaid, D. a. Krapchetov, D.M. Ford, Solubility-based gas separation with oligomer-modified inorganic membranes: Part III. Effects of synthesis conditions, J. Memb. Sci. 246 (2005) 181–191. doi:10.1016/j.memsci.2004.08.017.

[37] P. Li, M.R. Coleman, Synthesis of room temperature ionic liquids based random copolyimides for gas separation applications, Eur. Polym. J. 49 (2013) 482–491. doi:10.1016/j.eurpolymj.2012.11.016.

[38] S.-H. Pak, Y.-W. Jeon, M.-S. Shin, H.C. Koh, Preparation of Cellulose Acetate Hollow-Fiber Membranes for CO_2/CH_4 Separation, Environ. Eng. Sci. 33 (2015) ees.2015.0201. doi:10.1089/ees.2015.0201.

[39] H. Sanaeepur, B. Nasernejad, A. Kargari, Cellulose acetate/nano-porous zeolite mixed matrix membrane for CO_2 separation, Greenh. Gases Sci. Technol. 5 (2015) 291–304. doi:10.1002/ghg.1478.

[40] S. LOEB, S. SOURIRAJAN, Saline Water Conversion—II, in: Saline Water Conversion—II, AMERICAN CHEMICAL SOCIETY, WASHINGTON, D. C., 1963: pp. 117–132. doi:10.1021/ba-1963-0038.

[41] T.-S. Chung, S.K. Teoh, W.W.Y. Lau, M.P. Srinivasan, Effect of shear stress within the spinneret on hollow fiber membrane morphology and separation performance, Ind. Eng. Chem. Res. 37 (1998) 3930–3938. doi:10.1021/ie9802111.

[42] D.Y. Xing, N. Peng, T.S. Chung, Investigation of unique interactions between cellulose acetate and ionic liquid [EMIM]SCN, and their influences on hollow fiber ultrafiltration membranes, J. Memb. Sci. 380 (2011) 87–97. doi:10.1016/j.memsci.2011.06.032.

[43] J.T. Tsai, Y.S. Su, D.M. Wang, J.L. Kuo, J.Y. Lai, A. Deratani, Retainment of pore connectivity in membranes prepared with vapor-induced phase separation, J. Memb. Sci. 362 (2010) 360–373. doi:10.1016/j.memsci.2010.06.039.

[44] N. Peng, T.S. Chung, K.Y. Li, The role of additives on dope rheology and membrane formation of defect-free Torlon?? hollow fibers for gas separation, J. Memb. Sci. 343 (2009) 62–72. doi:10.1016/j.memsci.2009.07.010.

[45] C.Y. Feng, K.C. Khulbe, T. Matsuura, A.F. Ismail, Recent progresses in polymeric hollow fiber membrane preparation , characterization and applications, Sep. Purif. Technol. 111 (2013) 43–71. doi:10.1016/j.seppur.2013.03.017.

[46] A.L. Ahmad, Z.A. Jawad, S.C. Low, S.H.S. Zein, A cellulose acetate/multi-walled carbon nanotube mixed matrix membrane for CO_2/N_2 separation, J. Memb. Sci. 451 (2014) 55–66. doi:10.1016/j.memsci.2013.09.043.

[47] C.Y. Pan, Gas separation by high-flux, asymmetric hollow-fiber membrane, AIChE J. 32 (1986) 2020–2027. doi:10.1002/aic.690321212.

[48] L.A. Goetz, B. Jalvo, R. Rosal, A.P. Mathew, Superhydrophilic anti-fouling electrospun cellulose acetate membranes coated with chitin nanocrystals for water filtration, J. Memb. Sci. 510 (2016) 238–248. doi:10.1016/j.memsci.2016.02.069.

[49] W. gwi Kim, J.S. Lee, D.G. Bucknall, W.J. Koros, S. Nair, Nanoporous layered silicate AMH-3/cellulose acetate nanocomposite membranes for gas separations, J. Memb. Sci. 441 (2013) 129–136. doi:10.1016/j.memsci.2013.03.044.

[50] V.K. Thakur, S.I. Voicu, Recent advances in cellulose and chitosan based membranes for water purification: A concise review, Carbohydr. Polym. 146 (2016) 148–165. doi:10.1016/j.carbpol.2016.03.030.

[51] D.Y. Xing, N. Peng, T.S. Chung, Formation of cellulose acetate membranes via phase

inversion using ionic liquid, [BMIM][SCN], As the solvent, Ind. Eng. Chem. Res. 49 (2010) 8761–8769. doi:10.1021/ie1007085.

[52] J.E. Bara, E.S. Hatakeyama, C.J. Gabriel, X. Zeng, S. Lessmann, D.L. Gin, R.D. Noble, Synthesis and light gas separations in cross-linked gemini room temperature ionic liquid polymer membranes, J. Memb. Sci. 316 (2008) 186–191. doi:10.1016/j.memsci.2007.08.052.

[53] J. Albo, T. Yoshioka, T. Tsuru, Porous Al2O3/TiO2 tubes in combination with 1-ethyl-3-methylimidazolium acetate ionic liquid for CO2/N 2 separation, Sep. Purif. Technol. 122 (2014) 440–448. doi:10.1016/j.seppur.2013.11.024.

[54] A. Dahi, K. Fatyeyeva, D. Langevin, C. Chappey, S.P. Rogalsky, O.P. Tarasyuk, A. Benamor, S. Marais, Supported ionic liquid membranes for water and volatile organic compounds separation: Sorption and permeation properties, J. Memb. Sci. 458 (2014) 164–178. doi:10.1016/j.memsci.2014.01.031.

[55] E. Santos, J. Albo, A. Irabien, Acetate based Supported Ionic Liquid Membranes (SILMs) for CO_2 separation: Influence of the temperature, J. Memb. Sci. 452 (2014) 277–283. doi:10.1016/j.memsci.2013.10.024.

[56] Q. Gan, Y. Zou, D. Rooney, P. Nancarrow, J. Thompson, L. Liang, M. Lewis, Theoretical and experimental correlations of gas dissolution, diffusion, and thermodynamic properties in determination of gas permeability and selectivity in supported ionic liquid membranes., Adv. Colloid Interface Sci. 164 (2011) 45–55. doi:10.1016/j.cis.2011.01.005.

[57] G. Zarca, W.J. Horne, I. Ortiz, A. Urtiaga, J.E. Bara, Synthesis and gas separation properties

of poly(ionic liquid)-ionic liquid composite membranes containing a copper salt, J. Memb. Sci. 515 (2016) 109–114. doi:10.1016/j.memsci.2016.05.045.

[58] Z. Dai, R.D. Noble, D.L. Gin, X. Zhang, L. Deng, Combination of ionic liquids with membrane technology: A new approach for CO2 separation, J. Memb. Sci. 497 (2016) 1–20. doi:10.1016/j.memsci.2015.08.060.

[59] M.G. Cowan, M. Masuda, W.M. McDanel, Y. Kohno, D.L. Gin, R.D. Noble, Phosphonium-based poly(Ionic liquid) membranes: The effect of cation alkyl chain length on light gas separation properties and Ionic conductivity, J. Memb. Sci. 498 (2016) 408–413. doi:10.1016/j.memsci.2015.10.019.

[60] Y. Gu, T.P. Lodge, Synthesis and Gas Separation Performance of Triblock Copolymer Ion Gels with a Polymerized Ionic Liquid Mid-Block, Macromolecules. 44 (2011) 1732–1736. doi:10.1021/ma2001838.

[61] T.K. Carlisle, G.D. Nicodemus, D.L. Gin, R.D. Noble, CO_2/light gas separation performance of cross-linked poly(vinylimidazolium) gel membranes as a function of ionic liquid loading and cross-linker content, J. Memb. Sci. 397–398 (2012) 24–37. doi:10.1016/j.memsci.2012.01.006.

[62] P.T. Nguyen, B.A. Voss, E.F. Wiesenauer, D.L. Gin, R.D. Noble, Physically Gelled Room-Temperature Ionic Liquid-Based Composite Membranes for CO 2 / N 2 Separation : E ff ect of Composition and Thickness on Membrane Properties and Performance, (n.d.).

[63] L.C. Tomé, D. Mecerreyes, C.S.R. Freire, L.P.N. Rebelo, I.M. Marrucho, Pyrrolidinium-based polymeric ionic liquid materials: New perspectives for CO2 separation membranes,

J. Memb. Sci. 428 (2013) 260–266. doi:10.1016/j.memsci.2012.10.044.

[64] S. Spange, R. Lungwitz, A. Schade, Correlation of molecular structure and polarity of ionic liquids, J. Mol. Liq. 192 (2014) 137–143. doi:10.1016/j.molliq.2013.06.016.

[65] Cellulose Acetate, (n.d.). https://www.sigmaaldrich.com/catalog/product/aldrich/419028?lang=en&region=US.

[66] D. Morgan, L. Ferguson, P. Scovazzo, Diffusivities of Gases in Room-Temperature Ionic Liquids: Data and Correlations Obtained Using a Lag-Time Technique, Ind. Eng. Chem. Res. 44 (2005) 4815–4823. doi:10.1021/ie048825v.

[67] P. Scovazzo, D. Havard, M. McShea, S. Mixon, D. Morgan, Long-term, continuous mixed-gas dry fed CO_2/CH_4 and CO_2/N_2 separation performance and selectivities for room temperature ionic liquid membranes, J. Memb. Sci. 327 (2009) 41–48. doi:10.1016/j.memsci.2008.10.056.

[68] F. Sullivan-González, P. Scovazzo, R. Amos, S.-K. Bae, Hydrogen-bond acceptance's role in designing room temperature ionic liquid (RTIL) membranes for gas dehumidification, part I: Impacts on permeance and selectivity, J. Memb. Sci. 533 (2017) 190–200. doi:10.1016/j.memsci.2017.03.026.

[69] J. Sadlej, A. Jaworski, K. Miaskiewicz, A theoretical study of the vibrational spectra of imidazole and its different forms, J. Mol. Struct. 274 (1992) 247–257. doi:https://doi.org/10.1016/0022-2860(92)80161-A.

[70] A. Chowdhury, S.T. Thynell, Confined rapid thermolysis/FTIR/ToF studies of imidazolium-based ionic liquids, Thermochim. Acta. 443 (2006) 159–172.

doi:https://doi.org/10.1016/j.tca.2006.01.006.

[71] J. Dupont, On the solid, liquid and solution structural organization of imidazolium ionic liquids, J. Braz. Chem. Soc. 15 (2004) 341–350. http://www.scielo.br/scielo.php?script=sci_arttext&pid=S0103-50532004000300002&nrm=iso.

[72] E.J. Maginn, Molecular simulation of ionic liquids: current status and future opportunities, J. Phys. Condens. Matter. 21 (2009) 373101. doi:10.1088/0953-8984/21/37/373101.

[73] S. Satyen, H. Satoshi, K. Akiko, H. Hiro-o, Crystal Structure of 1-Butyl-3-methylimidazolium Chloride. A Clue to the Elucidation of the Ionic Liquid Structure, Chem. Lett. 32 (2003) 740–741. doi:10.1246/cl.2003.740.

[74] J.N.A. Canongia Lopes, A.A.H. Pádua, Nanostructural Organization in Ionic Liquids, J. Phys. Chem. B. 110 (2006) 3330–3335. doi:10.1021/jp056006y.

[75] S.A. Hashemifard, A.F. Ismail, T. Matsuura, Prediction of gas permeability in mixed matrix membranes using theoretical models, J. Memb. Sci. 347 (2010) 53–61. doi:10.1016/j.memsci.2009.10.005.

[76] H. Liu, S. Dai, D. Jiang, Molecular Dynamics Simulation of Anion Effect on Solubility, Diffusivity, and Permeability of Carbon Dioxide in Ionic Liquids, Ind. Eng. Chem. Res. 53 (2014) 10485–10490. doi:10.1021/ie501501k.

[77] M. Klähn, A. Seduraman, What Determines CO_2 Solubility in Ionic Liquids? A Molecular Simulation Study, J. Phys. Chem. B. 119 (2015) 10066–10078. doi:10.1021/acs.jpcb.5b03674.

[78] L. Ferguson, P. Scovazzo, Solubility, diffusivity, and permeability of gases in phosphonium-based room temperature ionic liquids: Data and correlations, Ind. Eng. Chem. Res. 46 (2007) 1369–1374. doi:10.1021/ie0610905.

[79] C.A. Scholes, S.E. Kentish, G.W. Stevens, Carbon Dioxide Separation through Polymeric Membrane Systems for Flue Gas Applications, Recent Patents Chem. Eng. 1 (2008) 52–66. doi:10.2174/2211334710801010052.

[80] C. Staudt-Bickel, W.J. Koros, Olefin/paraffin gas separations with 6FDA-based polyimide membranes, J. Memb. Sci. 170 (2000) 205–214. doi:10.1016/S0376-7388(99)00351-8.

[81] P. Cserjési, N. Nemestóthy, K. Bélafi-Bakó, Gas separation properties of supported liquid membranes prepared with unconventional ionic liquids, J. Memb. Sci. 349 (2010) 6–11. doi:10.1016/j.memsci.2009.10.044.

[82] H. Yang, Z. Xu, M. Fan, R. Gupta, R.B. Slimane, A.E. Bland, I. Wright, Progress in carbon dioxide separation and capture: A review, J. Environ. Sci. 20 (2008) 14–27.

[83] Y. Zhang, J. Sunarso, S. Liu, R. Wang, Current status and development of membranes for CO_2/CH_4 separation: A review, Int. J. Greenh. Gas Control. 12 (2013) 84–107.

[84] S. Sridhar, B. Smitha, T.M. Aminabhavi, Separation of carbon dioxide from natural gas mixtures through polymeric membranes — A review, Sep. Purif. Rev. 36 (2007) 113–174.

[85] P. Pandey, R.S. Chauhan, Membranes for gas separation, Prog. Polym. Sci. 26 (2001) 853–893.

[86] R.W. Baker, Future Directions of Membrane Gas Separation Technology, Ind. Eng. Chem. Res. 41 (2002) 1393–1411. doi:10.1021/ie0108088.

[87] H. Li, Z. Song, X. Zhang, Y. Huang, S. Li, Y. Mao, Ultrathin, Molecular-Sieving Graphene Oxide Membranes for Selective Hydrogen Separation, 1049 (2012) 95–98.

[88] M.A. Carreon, S. Li, J.L. Falconer, R.D. Noble, Alumina-supported SAPO-34 membranes for CO_2/CH_4 separation, J. Am. Chem. Soc. 130 (2008) 5412–5413.

[89] S.R. Venna, M.A. Carreon, Highly permeable zeolite imidazolate framework-8 membranes for CO_2/CH_4 separation, J. Am. Chem. Soc. 132 (2009) 76–78.

[90] M. Sevilla, A.B. Fuertes, CO_2 adsorption by activated templated carbons, J. Colloid Interface Sci. 366 (2012) 147–154. doi:10.1016/j.jcis.2011.09.038.

[91] S.-Y. Lee, S.-J. Park, Determination of the optimal pore size for improved CO_2 adsorption in activated carbon fibers., J. Colloid Interface Sci. 389 (2013) 230–5. doi:10.1016/j.jcis.2012.09.018.

[92] Y.S. Lin, Microporous and dense inorganic membranes: current status and prospective, Sep. Purif. Technol. 25 (2001) 39–55.

[93] R. Kumar, V.M. Suresh, T.K. Maji, C.N.R. Rao, Porous graphene frameworks pillared by organic linkers with tunable surface area and gas storage properties, Chem. Commun. 50 (2014) 2015–2017.

[94] K. Xia, X. Tian, S. Fei, K. You, Hierarchical porous graphene-based carbons prepared by carbon dioxide activation and their gas adsorption properties, Int. J. Hydrogen Energy. 39 (2014) 11047–11054.

[95] S. Mahmood Fatemi, M. Arabieh, H. Sepehrian, Nanoporous graphene oxide membrane and its application in molecular sieving, Carbon Lett. 16 (2015) 183–191.

doi:10.5714/CL.2015.16.3.183.

[96] Y. Tao, Q. Xue, Z. Liu, M. Shan, C. Ling, T. Wu, X. Li, Tunable hydrogen separation in porous graphene membrane: First-principle and molecular dynamic simulation, ACS Appl. Mater. Interfaces. 6 (2014) 8048–8058. doi:10.1021/am4058887.

[97] O. Leenaerts, B. Partoens, F.M. Peeters, Graphene: A perfect nanoballoon, Appl. Phys. Lett. 93 (2008) 193107. doi:10.1063/1.3021413.

[98] J.S. Bunch, S.S. Verbridge, J.S. Alden, A.M. Van Der Zande, J.M. Parpia, H.G. Craighead, P.L. Mceuen, Impermeable Atomic Membranes from 2008, (2008) 3–7.

[99] T. Wu, Q. Xue, C. Ling, M. Shan, Z. Liu, Y. Tao, X. Li, Fluorine-Modi fi ed Porous Graphene as Membrane for CO 2 / N 2 Separation : Molecular Dynamic and First-Principles Simulations, (2014). doi:Doi 10.1021/Jp4096776.

[100] G. Lei, C. Liu, H. Xie, F. Song, Separation of the hydrogen sulfide and methane mixture by the porous graphene membrane: Effect of the charges, Chem. Phys. Lett. 599 (2014) 127–132. doi:10.1016/j.cplett.2014.03.040.

[101] C. Sun, M.S.H. Boutilier, H. Au, P. Poesio, B. Bai, R. Karnik, N.G. Hadjiconstantinou, Mechanisms of molecular permeation through nanoporous graphene membranes, Langmuir. 30 (2014) 675–682. doi:10.1021/la403969g.

[102] H. Du, J. Li, J. Zhang, G. Su, X. Li, Y. Zhao, Separation of Hydrogen and Nitrogen Gases with Porous Graphene Membrane, J. Phys. Chem. C. 115 (2011) 23261–23266. doi:10.1021/jp206258u.

[103] D. Jiang, V.R. Cooper, S. Dai, Porous graphene as the ultimate membrane for gas

separation., Nano Lett. 9 (2009) 4019–24. doi:10.1021/nl9021946.

[104] L. Xu, M. Sahimi, T. Tsotsis, Nonequilibrium molecular dynamics simulations of transport and separation of gas mixtures in nanoporous materials, Phys. Rev. E. Stat. Phys. Plasmas. Fluids. Relat. Interdiscip. Topics. 62 (2000) 6942–8. doi:1063-651X/2000/62(5)/6942(7).

[105] H.W. Kim, H.W. Yoon, S.-M. Yoon, B.M. Yoo, B.K. Ahn, Y.H. Cho, H.J. Shin, H. Yang, U. Paik, S. Kwon, J.-Y. Choi, H.B. Park, Selective gas transport through few-layered graphene and graphene oxide membranes., Science. 342 (2013) 91–5. doi:10.1126/science.1236098.

[106] R.K. Joshi, P. Carbone, F.C. Wang, V.G. Kravets, Y. Su, I. V Grigorieva, H.A. Wu, A.K. Geim, R.R. Nair, Precise and ultrafast molecular sieving through graphene oxide membranes., Science. 343 (2014) 752–4. doi:10.1126/science.1245711.

[107] C. Chi, X. Wang, Y. Peng, Y. Qian, Z. Hu, J. Dong, D. Zhao, Facile Preparation of Graphene Oxide Membranes for Gas Separation, Chem. Mater. 28 (2016) 2921–2927. doi:10.1021/acs.chemmater.5b04475.

[108] K. Zahri, P.S. Goh, A.F. Ismail, The incorporation of graphene oxide into polysulfone mixed matrix membrane for CO_2/CH_4 separation, in: IOP Conf. Ser. Earth Environ. Sci., 2016: p. 12007. doi:10.1088/1755-1315/36/1/012007.

[109] P. Sun, M. Zhu, K. Wang, M. Zhong, J. Wei, D. Wu, Z. Xu, H. Zhu, Selective ion penetration of graphene oxide membranes, ACS Nano. 7 (2013) 428–437. doi:10.1021/nn304471w.

[110] D.R. Dreyer, S. Park, C.W. Bielawski, R.S. Ruoff, The chemistry of graphene oxide, Chem.

Soc. Rev. 39 (2010) 228–240.

[111] a. Peigney, C. Laurent, E. Flahaut, R.R. Bacsa, a. Rousset, Specific surface area of carbon nanotubes and bundles of carbon nanotubes, Carbon N. Y. 39 (2001) 507–514. doi:10.1016/S0008-6223(00)00155-X.

[112] J. Schrier, J. Schrier, Fluorinated and Nanoporous Graphene Materials As Sorbents for Gas Separations Gas Separations, 4458 (2011) 4451–4458.

[113] B. Yuan, X. Wu, Y. Chen, J. Huang, H. Luo, S. Deng, Adsorption of CO_2, CH_4, and N_2 on Ordered mesoporous carbon: Approach for greenhouse gases capture and biogas upgrading, Environ. Sci. Technol. 47 (2013) 5474–5480. doi:10.1021/es4000643.

[114] L. Lu, S. Wang, E.A. Müller, W. Cao, Y. Zhu, X. Lu, G. Jackson, Adsorption and separation of CO_2/CH_4 mixtures using nanoporous adsorbents by molecular simulation, Fluid Phase Equilib. 362 (2014) 227–234. doi:10.1016/j.fluid.2013.10.013.

[115] T.T. Trinh, K.-Q. Tran, Q.-V. Bach, D.Q. Trinh, A Molecular Dynamics Simulation Study on Separation Selectivity of CO_2/CH_4 Mixture in Mesoporous Carbons, Energy Procedia. 86 (2016) 144–149. doi:10.1016/j.egypro.2016.01.015.

[116] X. Peng, W. Wang, R. Xue, Z. Shen, Adsorption separation of CH_4/CO_2 on mesocarbon microbeads: Experiment and modeling, AIChE J. 52 (2006) 994–1003. doi:10.1002/aic.10723.

[117] T.T. Trinh, T.J.H. Vlugt, M.-B. Hägg, D. Bedeaux, S. Kjelstrup, Selectivity and self-diffusion of CO_2 and H_2 in a mixture on a graphite surface., Front. Chem. 1 (2013) 38. doi:10.3389/fchem.2013.00038.

[118] H. Cheng, G. Lei, Multilayer graphene nanostructure separate CO_2/CH_4 mixture: Combining molecular simulations with ideal adsorbed solution theory, Chem. Phys. Lett. 661 (2016) 31–35. doi:10.1016/j.cplett.2016.08.061.

[119] S. Gatica, A. Nekhai, A. Scrivener, Adsorption and Gas Separation of Molecules by Carbon Nanohorns, Molecules. 21 (2016) 662. doi:10.3390/molecules21050662.

[120] C. Sun, B. Bai, Gas diffusion on graphene surfaces, Phys. Chem. Chem. Phys. 19 (2017) 3894–3902. doi:10.1039/C6CP06267A.

[121] S. Jiao, Z. Xu, Selective gas diffusion in graphene oxides membranes: A molecular dynamics simulations study, ACS Appl. Mater. Interfaces. 7 (2015) 9052–9059. doi:10.1021/am509048k.

[122] J. Zhang, M.B. Clennell, D.N. Dewhurst, K. Liu, Combined Monte Carlo and molecular dynamics simulation of methane adsorption on dry and moist coal, Fuel. 122 (2014) 186–197. doi:10.1016/j.fuel.2014.01.006.

[123] H. Liu, S. Dai, D. Jiang, Insights into CO2/N2 separation through nanoporous graphene from molecular dynamics., Nanoscale. 5 (2013) 9984–7. doi:10.1039/c3nr02852f.

[124] F. Rahmani, S. Nouranian, M. Mahdavi, A. Al-Ostaz, Molecular simulation insights on the in vacuo adsorption of amino acids on graphene oxide surfaces with varying surface oxygen densities, J. Nanoparticle Res. 18 (2016) 320. doi:10.1007/s11051-016-3631-7.

[125] M. Mahdavi, F. Rahmani, S. Nouranian, Molecular simulation of pH-dependent diffusion, loading, and release of doxorubicin in graphene and graphene oxide drug delivery systems, J. Mater. Chem. B. 4 (2016) 7441–7451. doi:10.1039/C6TB00746E.

[126] S. Stankovich, D.A. Dikin, R.D. Piner, K.A. Kohlhaas, A. Kleinhammes, Y. Jia, Y. Wu, S.T. Nguyen, R.S. Ruoff, Synthesis of graphene-based nanosheets via chemical reduction of exfoliated graphite oxide, Carbon N. Y. 45 (2007) 1558–1565.

[127] B.D. Freeman, Basis of Permeability/Selectivity Tradeoff Relations in Polymeric Gas Separation Membranes, Macromolecules. 32 (1999) 375–380. doi:10.1021/ma9814548.

[128] Yuri Yampolskii, I. Pinnau, B. Freeman, Materials Science of Membranes for Gas and Vapor Separation, John Wiley & Sons, Ltd, 2006. doi:10.1002/047002903X.

[129] S. Plimpton, Fast parallel algorithms for short-range molecular dynamics, J. Comput. Phys. 117 (1995) 1–19.

[130] M.C. Payne, M.P. Teter, D.C. Allan, T.A. Arias, J.D. Joannopoulos, Iterative minimization techniques for ab initio total-energy calculations: molecular dynamics and conjugate gradients, Rev. Mod. Phys. 64 (1992) 1045.

[131] H. Sun, COMPASS: an ab initio force-field optimized for condensed-phase applications overview with details on alkane and benzene compounds, J. Phys. Chem. B. 102 (1998) 7338–7364.

[132] N. Grønbech-Jensen, N.R. Hayre, O. Farago, Application of the G-JF discrete-time thermostat for fast and accurate molecular simulations, Comput. Phys. Commun. 185 (2014) 524–527.

[133] J. Yang, Y. Ren, A. Tian, H. Sun, COMPASS force field for 14 inorganic molecules, He, Ne, Ar, Kr, Xe, H2, O2, N2, NO, CO, CO2, NO2, CS2, and SO2, in liquid phases, J. Phys. Chem. B. 104 (2000) 4951–4957.

[134] F. Rahmani, S. Nouranian, M. Mahdavi, J.H. O'Haver, A fundamental investigation of the surfactant-stabilized single-walled carbon nanotube/epoxy resin suspensions by molecular dynamics simulation, Mater. Res. Express. 4 (2017) 15016.

[135] T.T. Trinh, D. Bedeaux, J.-M. Simon, S. Kjelstrup, Calculation of the chemical potential and the activity coefficient of two layers of CO 2 adsorbed on a graphite surface, Phys. Chem. Chem. Phys. 17 (2015) 1226–1233. doi:10.1039/C4CP03782K.

[136] L.-L. Huang, Q. Shao, L.-H. Lu, X.-H. Lu, L.-Z. Zhang, J. Wang, S. Jiang, Helicity and temperature effects on static properties of water molecules confined in modified carbon nanotubes, Phys. Chem. Chem. Phys. 8 (2006) 3836. doi:10.1039/b604585p.

[137] O. Talu, A.L. Myers, Molecular Simulation of Adsorption : Gibbs Dividing Surface and Comparison with Experiment, AIChE J. 47 (2001) 1160–1168.

[138] T.T. Trinh, K.-Q. Tran, Q.-V. Bach, D.Q. Trinh, A Molecular Dynamics Simulation Study on Separation Selectivity of CO2/CH4 Mixture in Mesoporous Carbons, Energy Procedia. 86 (2016) 144–149. doi:10.1016/j.egypro.2016.01.015.

[139] T.T. Trinh, T.J.H. Vlugt, M.-B. Hägg, D. Bedeaux, S. Kjelstrup, Selectivity and self-diffusion of CO2 and H2 in a mixture on a graphite surface., Front. Chem. 1 (2013) 38. doi:10.3389/fchem.2013.00038.

[140] J. You, L. Tian, C. Zhang, H. Yao, W. Dou, B. Fan, S. Hu, Adsorption behavior of carbon dioxide and methane in bituminous coal: A molecular simulation study, Chinese J. Chem. Eng. 24 (2016) 1275–1282. doi:10.1016/j.cjche.2016.05.008.

[141] J. Zhang, K. Liu, M.B. Clennell, D.N. Dewhurst, Z. Pan, M. Pervukhina, T. Han, Molecular

simulation studies of hydrocarbon and carbon dioxide adsorption on coal, Pet. Sci. 12 (2015) 692–704. doi:10.1007/s12182-015-0052-7.

[142] S.G. Charati, S. a. Stern, Diffusion of Gases in Silicone Polymers: Molecular Dynamics Simulations, Macromolecules. 31 (1998) 5529–5535. doi:10.1021/ma980387e.

[143] H. Heller, M. Schaefer, K. Schulten, Molecular Dynamics Simulation of a Bilayer of 200 Lipids in the Gel and in the Liquid-Crystal Phases, J. Phys. Chem. B. 97 (1993) 8343–8360.

[144] M. V??gele, G. Hummer, Divergent Diffusion Coefficients in Simulations of Fluids and Lipid Membranes, J. Phys. Chem. B. 120 (2016) 8722–8732. doi:10.1021/acs.jpcb.6b05102.

[145] G. Arora, N.J. Wagner, S.I. Sandler, Adsorption and diffusion of molecular nitrogen in single wall carbon nanotubes., Langmuir. 20 (2004) 6268–6277. doi:10.1021/la036432f.

[146] D. Frenkel, B. Smit, Understanding molecular simulation: from algorithms to applications, Academic press, 2001.

[147] M. Shan, Q. Xue, N. Jing, C. Ling, T. Zhang, Z. Yan, J. Zheng, Influence of chemical functionalization on the CO2/N2 separation performance of porous graphene membranes, Nanoscale. 4 (2012) 5477. doi:10.1039/c2nr31402a.

[148] H. Lin, B.D. Freeman, Gas solubility, diffusivity and permeability in poly(ethylene oxide), J. Memb. Sci. 239 (2004) 105–117. doi:10.1016/j.memsci.2003.08.031.

LIST OF APPENDICES

APPENDIX A: CO_2 PPERMEABILITY AND SELECTIVITY

A.1. CO_2 Permeability and Selectivity Results

The permeabilities were determined using the steady state region of data. The pure gas permeabilities for CO_2, N_2, CH_4, and C_3H_8 were determined using initial pressures of approximately 30 kPa at 30°C (Table A.1).

The SILMs showed the highest permeability for the CO_2, while the dope membrane had the lowest permeable membrane for this gas.

Table A. 1. Experimental gas permeances in Barrers (1 Barrer = 10^{-10} $cm^3_{STP}.cm/(cm^2.s.cmHg)$) at 30°C.

Membrane	Permeability (Barrers)
	CO_2
Dope	179±2
CA/[emim][SCN]	196±5
SILM([emim][SCN])	217±7
SILM ([emim][Tf_2N])	1702.4 [a]
SILM ([emim][DCA])	1237.3 [a]
Polyimide membranes	17 [b]

[a] All data are determined from [6].

[b] All data are determined from [79].

[c] All data are determined from [80].

The separation selectivity of the CO_2/N_2 and CO_2/CH_4 is given in Table A.2. The selectivity of all the membranes can be similar due to the error associated with the selectivities. Therefore, no comments presented due to the similarity in the results.

Table A. 2. Experimental gas selectivities at 30°C.

Membrane	CO_2/N_2	CO_2/CH_4
Dope	24±8	9±2
CA/[emim][SCN]	30±10	14±3
SILM	37±8	19±3
SILM ([emim][Tf_2N])	23.1 [a]	12.2 [a]
SILM ([emim][DCA])	56.7 [a]	23 [a]
Polyimide membranes	36 [b]	20 [c]

[a] All data are determined from [6].

[b] All data are determined from [79].

[c] All data are determined from [148].

VITAE

Amir Khakpay

Address: 37 Rubin Drive, Oxford, MS 38655

Mobile: +1 662-380-2435

E-mail: akhakpay@go.olemiss.edu

Education

- **PhD:** *Chemical Engineering,* University of Mississippi*, Oxford, Mississippi, (2014 – 2017).*

  Thesis: **"Biphasic Cellulose Acetate/RTIL Membranes and Functionalized Graphene Adsorbents for Natural Gas Processing: Experimental and Molecular Simulation Studies".**

- **M.Sc.:** *Chemical Engineering,* University of Mississippi*, Oxford, Mississippi, (2014 – 2016).*

  Thesis: **"Investigation of the Effect of Polarity on the Ionic Liquids Permeability".**

- **M.Sc.:** *Chemical Engineering, Process Design,* University of Tehran*, Tehran, Iran, (2004 – 2006).*

Thesis: **"Investigation of the Effect of Surfactants on Mean Drops Size in the Mixer**

- **B.Sc.:** *Chemical Engineering, Process Design,* University of Tehran*, Tehran, Iran, (1999 – 2004).*

  Thesis: "Economical Investigation of Sulfur Coated Urea Production".

PUBLICATIONS:

PEER-REVIEWED JOURNAL PUBLICATIONS (13)

2018:

1. **Khakpay, A.,** Scovazzo, P. "Reverse-Selective Behavior of the Room Temperature Ionic Liquid Based Membranes for Natural Gas Processing." *Journal of Membrane Science* (2018), 545, pp 204–212.

   DOI: 10.1016/j.memsci.2017.09.068 (2015 ISI Impact Factor: 5.557).

2017:

2. **Khakpay, A.,** Rahmani, F., Nouranian, S., Scovazzo, P. "Molecular Insights on the CH_4/CO_2 Separation in Nanoporous Graphene and Graphene Oxide Separation Platforms: Adsorbents Versus Membranes." *The Journal of Physical Chemistry C* (2017), 121 (22), pp 12308–12320.

   DOI**:** 10.1021/acs.jpcc.7b03728 (2015 ISI Impact Factor: 4.509)

2015:

3. Ghorbanian, S. A., Davoudinejad, M., Radpour, S., **Khakpay, A.** "Modeling

Breakthrough Curves of Citric Acid Adsorption onto Anionic Resins in an Aqueous Solution." *The Journal of Engineering* (2015), 2015, pp 1–7.

DOI**:** 10.1155/2015/139041

2014:

4. Ghorbanian, S. A., Davoudinejad, M., Radpour, S., **Khakpay, A.** "Investigation of Breakthrough Curves of Citric Acid Adsorption." *Chemical and Biochemical Engineering Quarterly* (2014), 28 (3), pp 329-336.

   DOI**:** 10.15255/CABEQ.2013.1872 (2013 ISI Impact Factor: 0.911)

2013:

5. Salimi-Khorshidi, A, Abolghasemi, H., Kheirjooy, Z. **Khakpay, A.,** Esmaieli, M. "Spray and Packed Liquid-Liquid Extraction Columns: Drop Size and Dispersed Phase Mass Transfer." *Asia-Pacific Journal of Chemical Engineering* (2013), 8 (6), pp 940-949.

   DOI**:** 10.1002/apj.1739 (2011 ISI Impact Factor: 0.758)

6. Salimi-Khorshidi, A, Abolghasemi, H., **Khakpay, A.,** Younes-Sinaki, N. "Maximum Sauter Mean Diameter and Velocity of Drops in a Liquid-Liquid Spray Extraction Column." *Chemical and Biochemical Engineering Quarterly* (2013), 27 (3), pp 279-287.

   DOI**:** 10.15255/CABEQ.2013.108944 (2013 ISI Impact Factor: 0.911)

2011:

7. Sohbatzadeh-Lonbar, H., Abolghasemi, H., Ghannadi, M., **Khakpay, A.** "Investigation of Effective Parameters on Phase Inversion Holdup in Mixer Settler." *Nashrieh Takhassosie*

Daneshkade Mohandesie Shimi - University of Tehran (2011).

2010:

8. **Khakpay, A.,** Abolghasemi, H., Montazer-Rahmati, M. M. "The Effect of Sodium Dodecyl Sulfate on Mean Drop Size in a Horizontal Mixer Settler Extractor." *The Canadian Journal of Chemical Engineering* (2010), 88 (1), pp 101-108.
   DOI**:** 10.1002/cjce.20252 (2015 ISI Impact Factor: 1.066)

9. **Khakpay, A.,** Abolghasemi, H. "The Effects of Impeller Speed and Holdup on Mean Drop Size in a Mixer Settler with Spiral-Type Impeller, *The Canadian Journal of Chemical Engineering* (2010), 88 (3), pp 329-334.
   DOI**:** 10.1002/cjce.20287 (2015 ISI Impact Factor: 1.066)

2009:

10. **Khakpay, A.,** Abolghasemi, H., Salimi-Khorshidi, A "The Effects of a Surfactant on Mean Drop Size in a Mixer-Settler Extractor." *Chemical Engineering & Processing: Process Intensification* (2009), 48 (6), pp 1105-1111.
    DOI**:** 10.1016/j.cep.2009.02.003 (2015 ISI Impact Factor: 2.154)

11. Abolghasemi, H., **Khakpay, A.,** Kananpanah, S. "Investigating and Mathematical Correlating of the Presence Effect of Solute and Surfactant on Mean Drop Size in a Mixer-Settler." *Nashrieh Takhassosie Daneshkade Mohandesie Shimi - University of Tehran* (2009).

2008:

12. **Khakpay, A.,** Abolghasemi, H., Ghannadi, M., Sohbatzadeh-Lonbar, H. "Prediction and Modeling of Mean Drop Sizes in a Mixer-Settler Extractor and Comparing with Other Models." *Iranian Journal of Chemistry and Chemical Engineering* (2008).

13. Sohbatzadeh-Lonbar, H., Abolghasemi, H., Ghannadi, M., **Khakpay, A.** "Investigation of Phase Inversion Effect on Mass Transfer in a Continuous Mixer-Settler." *Iranian Journal of Chemistry and Chemical Engineering* (2008).

JOURNAL PUBLICATIONS (UNDER REVIEW OR IN PREPARATION) (7)

1. Ghorbanian, S. A., Bagheri, N.**, Khakpay, A.,** Pourkarimi, S. "Correlation with Different Models and a New Model for Adsorption Isotherms of Aniline, Benzaldehyde, and Benzoic Acid on Granular Activated Carbon." *Indian Journal of Chemical Technology (IJCT)* (2016) (Under Review). (2015 ISI Impact Factor: 0.491)

2. **Khakpay, A.,** Abolghasemi, H. "Mean Drop Size in Horizontal Mixer-Settler with a Spiral Impeller." *SCIREA Journal of Chemical Engineering* (2016) (Under Review).

3. Ghorbanian, S. A., Davoudinejad, M., Akbarpour-Tolouti, A.**, Khakpay, A.** "Prioritization of wastewater treatment processes in terms of energy production using Analytical Hierarchy Process." *Indian Journal of Research* (2016) (Under Review).

4. **Khakpay, A.,** Rahmani, F., Nouranian, S., Scovazzo, P. "Supported Ionic Liquid Membranes for Gas Separation: Experimental and Molecular Dynamic Simulation Study." (In Preparation).

5. **Khakpay, A.,** Rahmani, F., Nouranian, S., Scovazzo, P. "Molecular Dynamic Study of

Reverse-Selective Potential of the Supported Ionic Liquid Membranes." (In Preparation).

6. **Khakpay, A.,** Scovazzo, P., Nouranian, S. "Room Temperature Ionic Liquid Membranes Biphasic Membranes for Natural Gas Upgrading." (In Preparation).
7. **Khakpay, A.,** Scovazzo, P., Nouranian, S. "Novel Carbon-Carbon Membranes for Gas Separation." (In Preparation).

CONFERENCE PRESENTATIONS (13)

2017:

1. Rahmani, F., **Khakpay, A.,** Nouranian, S., Scovazzo, P. "CH_4 and CO_2 Transport Properties through Nanoporous Graphene and Graphene Oxide Membranes: A Molecular Dynamics Simulation Study." Abstract submitted to the 2017 Annual Meeting of the American Institute of Chemical Engineers (AIChE), Minneapolis, MN, U.S.A. October 29-November 3 (2017).
2. **Khakpay, A.,** Rahmani, F., Nouranian, S., Scovazzo, P. "Molecular Insights on the Reverse-Selectivity Potential of Room Temperature Ionic Liquid Membranes." Abstract submitted to the 2017 Annual Meeting of the American Institute of Chemical Engineers (AIChE), Minneapolis, MN, U.S.A. October 29-November 3 (2017).
3. Rahmani, F., **Khakpay, A.,** Nouranian, S., Scovazzo, P. "Molecular Dynamics Simulation of Room Temperature Ionic Liquid Membranes for CO_2/CH_4 and CO_2/N_2 Separations." Abstract submitted to the 2017 Annual Meeting of the American Institute of Chemical Engineers (AIChE), Minneapolis, MN, U.S.A. October 29-November 3 (2017).

2016:

4. **Khakpay, A.,** Scovazzo, P. "Reverse-Selective Behavior of the Room Temperature Ionic Liquid Based Membranes." The 2016 Annual Meeting of the American Institute of Chemical Engineers (AIChE), San Francisco, CA, U.S.A. November 13-18 (2016).

5. **Khakpay, A.,** Scovazzo, P., Nouranian, S. "Gas Separation Using Novel Carbon/Carbon Nanotube Composite Membranes." The 2016 Annual Meeting of the American Institute of Chemical Engineers (AIChE), San Francisco, CA, U.S.A. November 13-18 (2016).

2012:

6. Ghorbanian, S. A., Bagheri, N., **Khakpay, A.** "Investigation of Adsorption Isotherms of Benzaldehyde on Activated Carbon." The 1st National Conference on Industrial Water and Wastewater Treatment, Mahshahr, Khuzestan, Iran November 5-8 (2012).

7. Ghorbanian, S. A., Bagheri, N., **Khakpay, A.** "Investigation of Adsorption Isotherms of Benzoic Acid on Activated Carbon." The 1st National Conference on Industrial Water and Wastewater Treatment, Mahshahr, Khuzestan, Iran November 5-8 (2012).

8. Ghorbanian, S. A., Bagheri, N., **Khakpay, A.** "Investigation of Adsorption Isotherms of Aniline on Activated Carbon." The 1st National Conference on Industrial Water and Wastewater Treatment, Mahshahr, Khuzestan, Iran November 5-8 (2012).

2008:

9. Salimi-Khorshidi, A, Abolghasemi, H., **Khakpay, A.** "Correlating of Mean Drop Size in a Spray Extraction Column." The 12th Iranian Chemical Engineering Congress, Tabriz,

Eastern Azarbaijan, Iran November 10-15 (2008).

10. Abolghasemi, H., Kheirjooy, Z., Salimi-Khorshidi, A, **Khakpay, A.** "Determining and Correlating of Continuous Phase Sherwood Number in a Randomly Packed Extraction Column." The 12th Iranian Chemical Engineering Congress, Tabriz, Eastern Azarbaijan, Iran November 10-15 (2008).

2008:

11. **Khakpay, A.,** Abolghasemi, H., Ghannadi, M., Sohbatzadeh-Lonbar, H. "Investigation of Effects of Holdup and Impeller Speed on Drop Sizes in a Mixer-Settler." The 11th Iranian Chemical Engineering Congress, Tehran, Tehran, Iran November 9-14 (2008).

12. Sohbatzadeh-Lonbar, H., Abolghasemi, H., Ghannadi, M., **Khakpay, A.** "Investigation of the Physical Properties Effect on Phase Inversion in a Mixer-Settler." The 11th Iranian Chemical Engineering Congress, Tehran, Tehran, Iran November 9-14 (2008).

13. Sohbatzadeh-Lonbar, H., Abolghasemi, H., Ghannadi, M., **Khakpay, A.** "Investigation of Solute Concentration on Phase Inversion in a Mixer-Settler." The 11th Iranian Chemical Engineering Congress, Tehran, Tehran, Iran November 9-14 (2008).

Teaching Experience

- Teacher Assistant in the **Unit Operations Lab**, University of Mississippi, Oxford, Mississippi, USA, (2014 – 2017).
- Teacher, in **Process Simulation Using Hyprotech Software**, Valie Asr Boarding-School, 2006.
- Teacher, in **Process Control in Chemical Engineering**, Valie Asr Boarding-School, 2006.
- Teacher Assistant in the **Process Control in Chemical Engineering**, University of Tehran, Tehran, Iran. (2004 – 2006).
- Teacher, Applied Mathematics in Chemical Engineering, Mass Transfer, Kinetics and Reactor Design (2006 – 2013).